

# A Resolved Census of Millimeter Emission from Taurus Multiple Star Systems

Robert J. Harris, Sean M. Andrews, David J. Wilner

*Harvard-Smithsonian Center for Astrophysics, 60 Garden Street, Cambridge, MA 02138*

and

Adam L. Kraus<sup>1</sup>

*University of Hawaii Institute for Astronomy, 2680 Woodlawn Drive, Honolulu, HI 96822*

## ABSTRACT

We present a high angular resolution millimeter-wave dust continuum imaging survey of circumstellar material associated with the individual components of 23 multiple star systems in the Taurus-Auriga young cluster. Combined with previous measurements in the literature, these new data permit a comprehensive look at how the millimeter luminosity (a rough tracer of disk mass) relates to the separation and mass of a stellar companion. Approximately one third (28-37%) of the individual stars in multiple systems have detectable millimeter emission, an incidence rate half that for single stars ( $\sim 62\%$ ) which does not depend on the number of companions. There is a strong, positive correlation between the luminosity and projected separation ( $a_p$ ) of a stellar pair. Wide pairs ( $a_p > 300$  AU) have a similar luminosity distribution as single stars, medium pairs ( $a_p \approx 30$ -300 AU) are a factor of 5 fainter, and close pairs ( $a_p < 30$  AU) are  $\sim 5\times$  fainter yet (aside from a small, but notable population of bright circumbinary disks). In most cases, the emission is dominated by a disk around the primary (or a wide tertiary in hierarchical triples), but there is no clear relationship between luminosity and stellar mass ratio. A direct comparison of resolved disk sizes with predictions from tidal truncation models yields mixed results; some disks are much larger than expected given the projected distances of their companions. We suggest that the presence of a stellar companion impacts disk properties at a level comparable to the internal evolution mechanisms that operate in an isolated system, with both the multiple star formation process itself and star-disk tidal interactions likely playing important roles in the evolution of circumstellar material. From the perspective of the mass content of the disk reservoir, we expect that (giant) planet formation is inhibited around the components of close pairs or secondaries, but should be as likely as for single stars around the primaries (or wide tertiaries in hierarchical triples) in more widely-separated multiple star systems.

*Subject headings:* binaries — protoplanetary disks — stars: formation

---

<sup>1</sup>Hubble Fellow.

## 1. Introduction

Many, if not most, stars are born with close companions (Abt & Levy 1976; Duquennoy & Mayor 1991; Fischer & Marcy 1992; Raghavan et al. 2010, but see Lada 2006). Depending on their orbits, tidal interactions between individual stellar components in these multiple systems can dominate the evolution of their natal circumstellar material and potentially have drastic consequences for the planet formation process (e.g., Papaloizou & Pringle 1977; Lin & Papaloizou 1979a,b; Artymowicz & Lubow 1994). But even in these hazardous dynamical environments, many young multiples harbor long-lived circumstellar material (see Duchêne et al. 2007) and a growing number of their more mature counterparts are being identified as exoplanet hosts (e.g., Patience et al. 2002; Raghavan et al. 2006; Desidera & Barbieri 2007; Doyle et al. 2011). Given the prevalence of stellar multiplicity, an improved empirical understanding of the dynamical interplay between the stars and disks in these systems – including effects like tidal truncation, stripping, and the orbital evolution of companions – is fundamental for the development of a comprehensive model for the formation of stars and planetary systems. Moreover, constraints on these dynamical processes in multiple star systems can be used as high mass-ratio touchstones for theoretical work on analogous disk-planet interactions, particularly the creation of tidal gaps and subsequent planet migration.

A wealth of theoretical work suggests that the fate of the circumstellar material in a young multiple star system is primarily dependent on the separation ( $a$ ) and mass ratio ( $q$ ) of the individual components, as well as the orbital eccentricity ( $e$ ) (e.g., Artymowicz & Lubow 1994). Systems with eccentric orbits have an enhanced likelihood of star-disk tidal interactions. For a given orbit, a near equal-mass companion ( $q \sim 1$ ) should have a more destructive impact on disk material than a low-mass companion. But in most cases, the effects of  $\{e, q\}$  on the circumstellar material are secondary to the orbital separation. Systems with large separations ( $a \sim$  hundreds of AU) should impart little or no dynamical effects on their circumstellar material, leaving disks around each stellar component that are similar to those around single stars. Conversely, individual disks in a small-separation ( $a \sim$  a few AU or less) system will likely not survive. Instead, these systems can host a circum-multiple disk with a dynamically cleared central cavity out to a radius comparable to the stellar separation ( $\sim 2-3a$ ). However, most multiple systems both in the field and in young clusters have intermediate separations ( $a \sim$  tens of AU; Mathieu et al. 2000). The disks in these systems may suffer the most dramatic effects of star-disk interactions, resulting in their external truncation at a fraction of the component separation ( $\sim 0.2-0.5a$ ), or their complete dispersal.

Qualitatively, these theoretical predictions find some observational support. Statistical analyses of warm gas and dust diagnostics (accretion signatures and/or a near-infrared excess) indicate that the presence of a companion with separation  $\lesssim 40$  AU may significantly hasten disk dispersal near the stars (on  $\sim 1-10$  AU scales; Cieza et al. 2009; Kraus et al. 2012). This diminished frequency of disk signatures for “close” multiples was first noted at (sub)millimeter wavelengths by Jensen et al. (1994), and later confirmed in surveys of increasing size and sensitivity to dust emission (Osterloh & Beckwith 1995; Jensen et al. 1996b; Andrews & Williams 2005). Since the con-

tinuum emission at such long wavelengths is primarily optically thin (e.g., Beckwith et al. 1990), the systematically lower millimeter-wave luminosities from close multiples compared to systems with wider separations or single stars were taken as compelling evidence for decreased disk masses due to tidal truncation or disruption. However, that evidence is indirect: those observations relied on single-dish photometers that do not resolve the individual stellar components nor their disks. A quantitative investigation of the theory of star-disk interactions requires observations that can address how disk masses and sizes depend on the properties of the stellar system (particularly  $a$  and  $q$ ). With the right combination of angular resolution and mass sensitivity, interferometric measurements of the optically-thin millimeter continuum emission from the dusty disks in these systems are uniquely qualified for that task. Aside from a small collection of systems (e.g., Jensen et al. 1996a; Akeson et al. 1998; Jensen & Akeson 2003; Patience et al. 2008), such data are rare.

In this article, we present a Submillimeter Array (SMA) survey of the millimeter-wave continuum emission from 23 young multiple star systems in the Taurus-Auriga star formation region. These data represent the most comprehensive resolved census of cool dust emission from the disks that reside in young multiple systems to date. The motivation for the survey sample is introduced in §2, and the observations and data calibration are reviewed in §3. A simple modeling analysis of these data is conducted in §4, with a focus on retrieving luminosities and sizes from individual disks whenever possible. The results of this imaging survey are synthesized with other information in the literature in §4 to extract a statistically representative view of circumstellar material in multiple star systems. Based on that analysis, we attempt to reconcile the observations with theoretical predictions from tidal interaction models in §5. Finally, our key conclusions are summarized in §6.

## 2. The Sample

Multiplicity searches in the Taurus molecular clouds have a long history of success with a variety of techniques, ranging from straightforward direct imaging (Reipurth & Zinnecker 1993; White & Ghez 2001; Correia et al. 2006; Kraus & Hillenbrand 2009b) and radial velocity monitoring (e.g., Mathieu et al. 1997) to more specialized methods like lunar occultations (Simon et al. 1992, 1995; Richichi et al. 1999), speckle interferometry (Ghez et al. 1993; Leinert et al. 1993), and most recently aperture-mask interferometry (Kraus et al. 2011). There is now a reasonably complete census of Taurus multiple systems that have angular separations  $\rho \approx 0.03\text{--}30''$ ,  $K$ -band contrast ratios of  $\leq 6$  magnitudes ( $\leq 4$  mags for the systems with the smallest separations), and primary spectral types between F0 and M4. Assuming a mean distance of 145 pc (Loinard et al. 2007; Torres et al. 2007, 2009) and a crude estimation of stellar masses (see Kraus et al. 2011), this region of multiplicity parameter-space corresponds to projected separations  $a_p \approx 5\text{--}5000$  AU, stellar mass ratios  $q \approx 0.1\text{--}1.0$  (well into the brown dwarf regime), and primary star masses  $M_p \sim 0.2\text{--}2 M_\odot$ . There are currently 71 such multiple “systems” known in Taurus, consisting of 111 “pairs” of 179 individual stars. For the sake of clarity, we adopt a simple nomenclature in this article such that a “system” refers to any group of associated stars and a “pair” is meant as any subset of the

system that could potentially interact dynamically. A simple binary (2 stars) counts as 1 system and 1 pair. In a higher-order hierarchical multiple like UZ Tau, we consider the 4 stars UZ Tau Ea, Eb, Wa, and Wb to comprise 1 system of 3 pairs based on their relative projected separations: Ea–Eb, Wa–Wb, and Eab–Wab (i.e., this phenomenological scheme implicitly assumes that pairs like Ea–Wa are unlikely to interact directly: all such pairs are listed in §5).

The selection criteria for our resolved millimeter-wave imaging survey were motivated by practical observational limitations and consist of two requirements: (1) a composite system flux density of  $\geq 20$  mJy at  $880 \mu\text{m}$ , and (2) an angular separation of  $\geq 0''.3$  for at least one pair in the system. The first criterion is a sensitivity restriction that would ensure that our observations could firmly detect ( $3\text{--}5\sigma$ ) two equivalent disks around individual stellar components with the typical expected RMS sensitivity of  $\sim 2\text{--}3$  mJy beam $^{-1}$  (see §3). Flux density estimates for unresolved systems were compiled from the single-dish survey of Andrews & Williams (2005). If no suitable  $880 \mu\text{m}$  flux density was available, the 1.3 mm measurements of Beckwith et al. (1990) or Osterloh & Beckwith (1995) were scaled up by a conservative factor of  $(1.3/0.88)^2 \approx 2.2$  based on the median emission ratio at those wavelengths (Andrews & Williams 2005, 2007a). Note that for the standard optically thin and isothermal assumptions for converting luminosity into mass, this sensitivity threshold corresponds to  $\sim 5 M_{\oplus}$  of dust (or a total mass of  $\sim 1.5 M_{\text{Jup}}$  for a 100:1 gas-to-dust mass ratio). The second criterion is a resolution restriction set by the longest available baselines of the SMA ( $\sim 0.5$  km) that ensures we would be able to resolve the individual stellar components of a given pair. Only systems where the angular separations of all its constituent pairs are  $< 0''.3$  were excluded. The resulting sample includes systems where some pair has a projected separation  $a_p > 40$  AU.

Of the original 71 systems, 29 exceed the  $880 \mu\text{m}$  luminosity selection threshold. Of those 29 systems, only 2 fail to meet the resolution criterion (IS Tau and DQ Tau; the latter is a spectroscopic binary). The resulting 27 systems are comprised of 52 pairs and a total of 77 individual stars. We elected not to observe 4 of those systems with the SMA (FS Tau/Haro 6-5B, XZ/HL Tau, FZ/FY Tau, and V807/GH Tau) because their wide-separation pairs were already resolved with single-dish telescopes and their remaining pairs were too faint or too close to meet our selection criteria. The systems in our  $880 \mu\text{m}$  flux- and resolution-limited sample are listed in Table 1.

Given the practical restrictions that were imposed in its construction, it is important to investigate the resulting sample for unintended biases. Since our selection criteria do not specifically address the stellar masses in these systems, the key potential biases could be related to the mass ratios of pairs ( $q$ ), the “primary” masses ( $M_p$ ; meaning the mass of the brighter component of a pair), or the total pair masses (the sum of the primary and secondary components of a pair,  $M_{\text{pair}} = M_p + M_s$ ). Figure 1 directly compares the cumulative distributions of  $q$ ,  $M_p$ , and  $M_{\text{pair}}$  for the pairs included in our sample (*black*) against those that were excluded due to their low millimeter luminosities and/or small angular separations (*gray*). Note that masses were typically determined from the Baraffe et al. (1998) models by Kraus et al. (2011); complete references are provided in §5. A two-sided Kolmogorov-Smirnov (K-S) test confirms that our sample is not biased with respect to  $q$  or  $M_p$ , with probabilities that the sample multiples and other multiples are drawn from the same

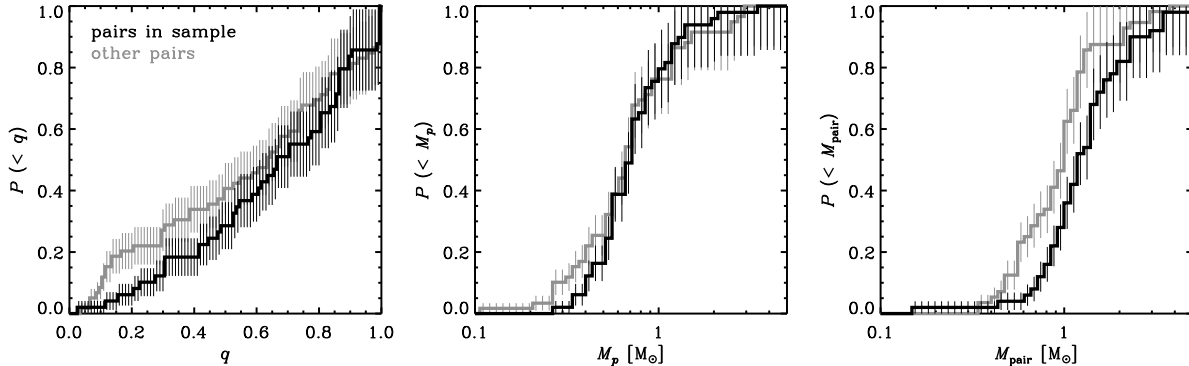


Fig. 1.— A comparison of the cumulative distributions of the stellar mass ratios ( $q$ ), primary masses ( $M_p$ ), and composite pair masses ( $M_{\text{pair}} = M_p + M_s$ ) between the systems that were selected (*black*) and excluded (*gray*) from our sample. While our selection criteria do not produce a significant bias in  $q$  or  $M_p$ , they tend to include pairs with marginally higher *total* stellar masses ( $M_{\text{pair}}$ ).

parent distributions of mass ratios or primary masses being  $\sim 73\%$  and  $20\%$ , respectively. However, the distribution of  $M_{\text{pair}}$  for the pairs in our sample are found to be drawn from a marginally different – and systematically *higher* – parent distribution than their counterparts that were not selected, with a K-S probability of only  $2\%$  (although it is worthwhile to keep in mind that these individual stellar mass estimates are crude).

### 3. Observations and Data Reduction

The 23 multiple systems listed in Table 1 (not including the additional 4 systems in italics; see §2) were observed with the SMA interferometer (Ho et al. 2004) in a variety of observing configurations and receiver settings over the past 6 years, with most of the data obtained in the past 20 months. An observing log is provided in Table 2. All systems were observed in the compact (C) array configuration, with baseline lengths of 8-70 m. Additional measurements were made with the extended (E: 28-226 m baselines) or very extended (V: 68-509 m baselines) configurations for the systems that contain pairs with smaller angular separations. Some of these data were presented in previous work (Andrews & Williams 2007b; Andrews et al. 2011). All but 4 of these 23 systems were observed with the 345 GHz receivers: the pairs in the HP Tau, GI/GK Tau, MHO 1/2, and GG Tau systems that we aimed to probe have wide enough separations that they were instead observed with slightly lower resolution at 230 GHz. We made some additional observations of systems that were *not* in our sample, since they had not yet been observed at millimeter wavelengths (see §5).

In most cases, the SMA dual-sideband receivers were tuned to a local oscillator (LO) frequency of 340.755 GHz ( $880 \mu\text{m}$ ) or 225.497 GHz ( $1.3 \text{ mm}$ ). Some tracks used shifted LO settings to accommodate other projects that shared one night of observing. The data obtained in 2010-2011 employs two IF bands (per sideband) spanning  $\pm 4\text{-}6 \text{ GHz}$  and  $\pm 6\text{-}8 \text{ GHz}$  from the LO frequency (only

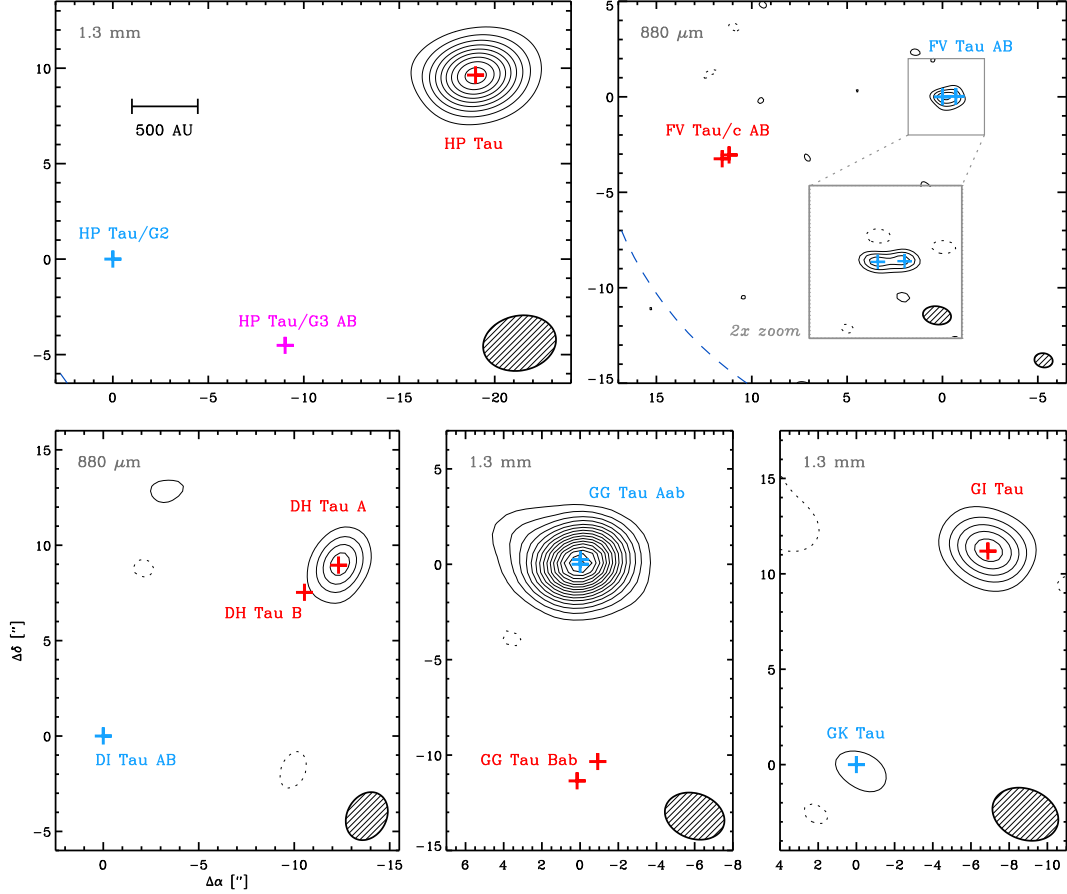


Fig. 2.— Mosaic of SMA continuum images for wide-separation multiple systems. Contours are drawn at  $3\sigma$  intervals (see Table 3); hatched ellipses mark the synthesized beam dimensions. Stellar positions are marked with blue (primary), red (secondary), or purple (intermediate mass in higher-order systems) crosses. A blue dashed curve marks the SMA primary beam in the FV Tau map. The FV Tau inset shows the data synthesized at higher resolution, with a beam size of  $0''.7 \times 0''.5$ . The panels are drawn to scale; a 500 AU scale bar is marked in the HP Tau system panel (*top left*).

the lower IF band was available for the 2 observations in 2005 and 2009). Each IF band contains 24 partially overlapping 108 MHz-wide spectral chunks (per sideband). Aside from one chunk reserved for the local CO transition, each of these was coarsely divided into 32 channels to observe the continuum. A finer sampling of 256 channels per chunk was used to probe the CO emission, corresponding to a velocity resolution of 0.40 and 0.55  $\text{km s}^{-1}$  near the  $J=3-2$  and  $J=2-1$  transitions, respectively. The observations cycled between various target systems and the nearby quasars 3C 111 and J0510+180 on timescales of  $\sim 20$  minutes for the compact array and 10 minutes for the longer baseline configurations. Bright quasars (3C 279 or 3C 454.3), Uranus, and satellites (Titan, Callisto) were observed as bandpass and absolute amplitude calibrators when the targets

were at low elevations. Observing conditions were often excellent, with precipitable water vapor levels ranging from 1.0-1.6 mm and  $\sim 2$ -3 mm for the 880  $\mu$ m and 1.3 mm observations, respectively.

The data were reduced with the IDL-based MIR software package. The spectral response was calibrated using observations of bright quasars as references, and the central 82 MHz from the individual spectral chunks in each sideband and IF band were averaged into an effective continuum channel (excluding the chunk containing a CO transition). The antenna-based complex gain response of the system was determined using the phase calibrator nearest to the target. The absolute amplitude scale was set based on observations of Uranus or planetary satellites, and is expected to be accurate at the level of  $\sim 10\%$ . For each target, the continuum channels for both IF bands and sidebands from each set of observations were combined into a composite set of calibrated visibilities. The MIRIAD software package was used to Fourier invert those visibilities, perform a deconvolution using the CLEAN algorithm, and restore the CLEANed maps with a synthesized beam. The synthesized beam dimensions and RMS noise levels for the naturally weighted datasets are provided in Table 3. The SMA continuum maps are shown in Figures 2-4. In most cases, the observations of a given multiple system were not sufficient to clearly detect CO emission from any circumstellar gas: the few exceptions will be discussed elsewhere.

#### 4. Disk Properties from Simple Emission Models

The SMA survey observations described above comprise the largest resolved millimeter-wave census of circumstellar material in young multiple star systems to date. In this section, we aim to measure two fundamental properties from these data – luminosities (which are related to dust masses) and sizes – for the disks around the individual stellar components in each multiple system. These basic disk parameters are estimated by fitting a simple model of the continuum emission morphology directly to the observed visibilities. The 27 multiple systems in our sample contain 77 individual stars. The available data have sufficient angular resolution to associate any dust emission with 50 of those stars. The individual components in the close pairs MHO 2 AB, T Tau Sab, FS Tau AB, DI Tau AB, UX Tau Bab, XZ Tau AB, GG Tau Aab, UZ Tau Eab, V807 Tau AB, GH Tau AB, HP Tau/G3 AB, HV Tau AB, and Haro 6-37 Aab are not resolved. We treat the millimeter signal from each of these 13 pairs as if it arises from a “composite” disk (see §5.1).

Including two of those composites, there are 14 individual disks in this sample that are sufficiently well-resolved to provide robust estimates of their basic parameters. In these cases, we define a simple, azimuthally symmetric and geometrically flat emission model with a power-law radial surface brightness distribution,  $I_\nu \propto R^{-x}$ , that extends to an outer edge,  $R_d$ . The emission profile is normalized such that the total flux density  $F_d = \int I_\nu d\Omega$ . This parametric emission morphology is designed to mimic what would be expected from a disk structure model with power-law surface density ( $\Sigma_d \propto R^{-p}$ ) and temperature ( $T_d \propto R^{-q}$ ) profiles. Pressing that resemblance, the radial index  $x$  is analogous to the sum  $p+q$  and the normalization  $F_d$  is a rough proxy for the product  $\kappa_d \langle T_d \rangle M_d$ , where  $\kappa_d$  is the dust opacity,  $\langle T_d \rangle$  is a characteristic temperature, and  $M_d$  is the dust mass, mod-

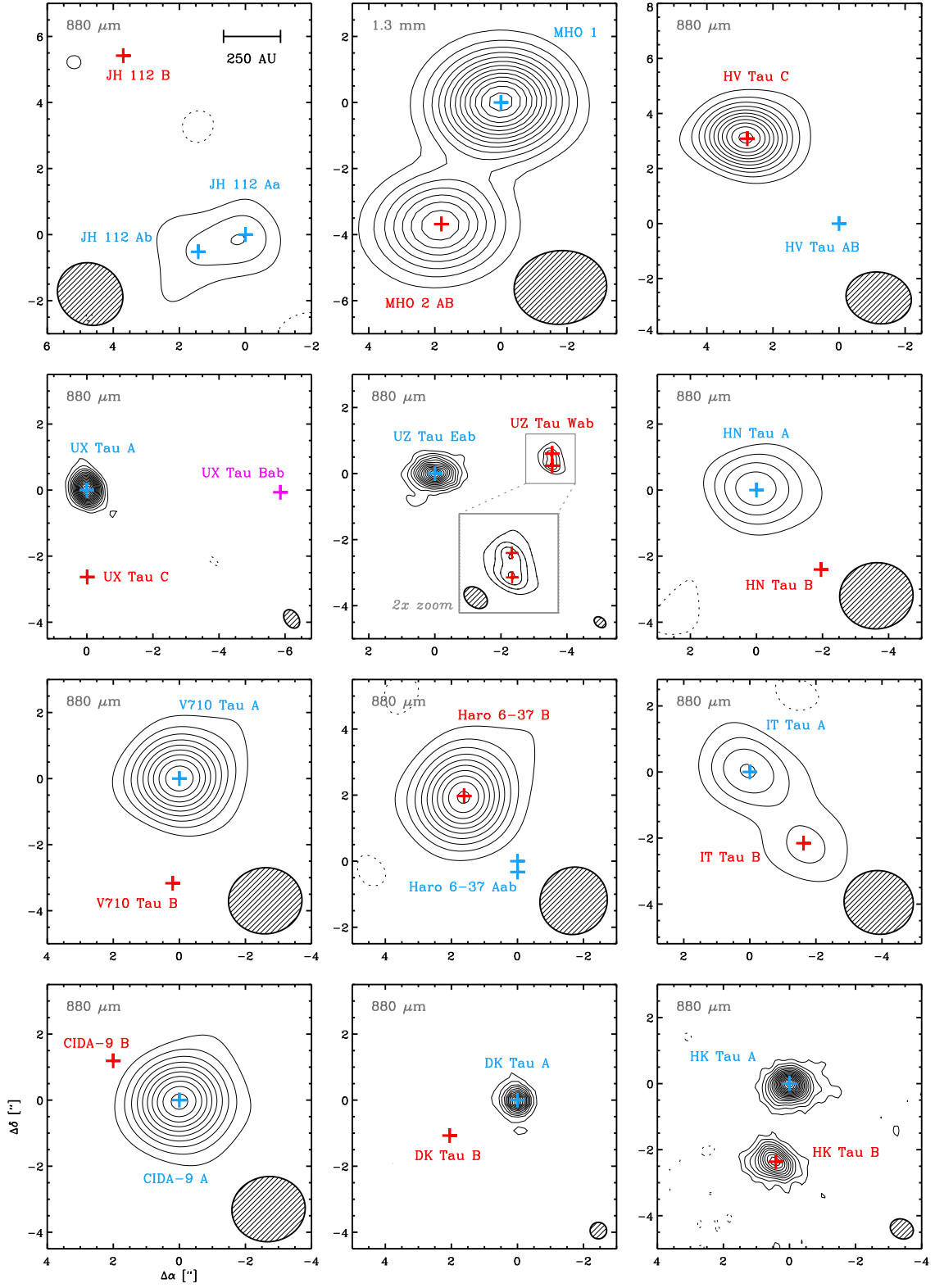


Fig. 3.— Same as Fig. 2, for medium separations.



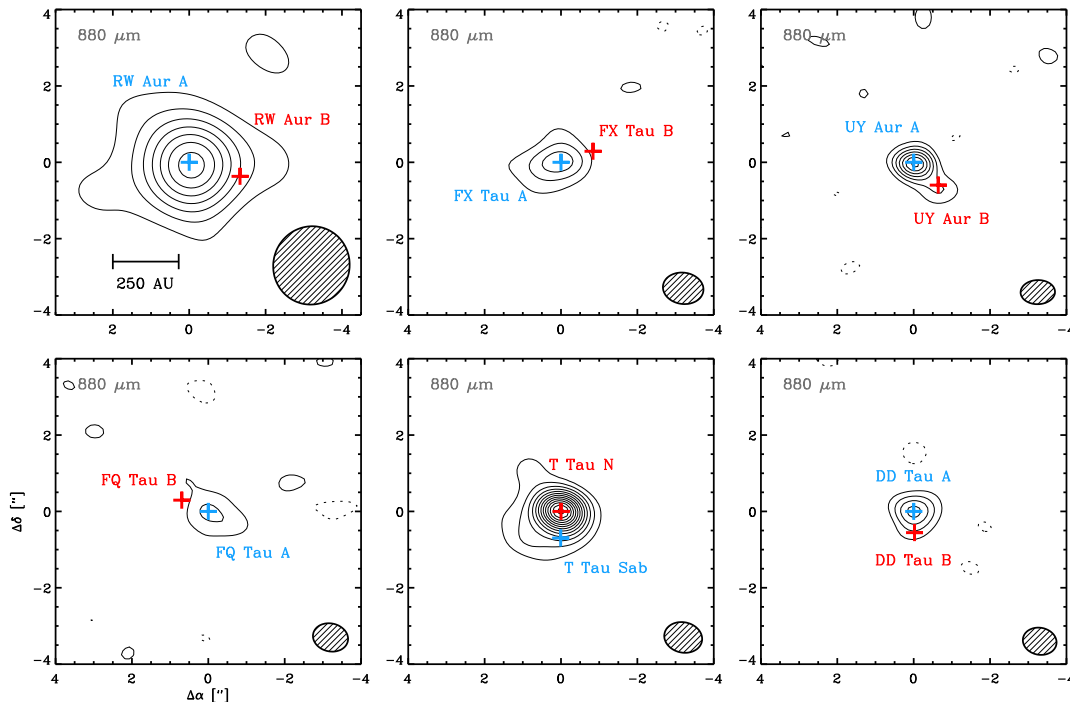


Fig. 4.— Same as Figs. 2 and 3, for small separations.

ulo small correction factors for any high optical depths in the disk center (Beckwith et al. 1990; Andrews & Williams 2005). Our data do not generally have enough sensitivity on long baselines to provide useful quantitative constraints on both the emission gradient and size, which are effectively degenerate at this modest resolution (see Mundy et al. 1996; Andrews & Williams 2007b). Since the key parameters of interest from the perspective of tidal interaction models are  $\{F_d, R_d\}$ , we elect to fix the gradient to a fiducial value,  $x = 1.5$ , motivated by the standard assumptions for irradiated accretion disks ( $p = 1, q = 0.5$ ; see Hartmann et al. 1998). For reference, adjustments to the radial index of  $\pm 30\%$  ( $\Delta x \approx \pm 0.5$ ) induce systematic changes in the size estimates of  $\sim 20\text{-}40\%$ : steeper (shallower) gradients produce larger (smaller) sizes.

In addition to the two free parameters in the surface brightness model,  $\{F_d, R_d\}$ , there are formally five other parameters related to the projection of the model into the sky plane: the disk center relative to the observed phase center  $\{\Delta\alpha, \Delta\delta\}$ , the disk viewing geometry described by its apparent inclination and orientation  $\{i_d, \text{PA}_d\}$ , and the distance to the observer  $\{d\}$ . The latter is fixed to  $d = 145$  pc, with a systematic uncertainty estimated to be roughly  $\pm 10\%$  (Loinard et al. 2007; Torres et al. 2007, 2009). We fix the centroid positions before estimating other parameters, typically based on an elliptical Gaussian fit to the visibilities for individual components that exhibit continuum emission. In general, that technique recovers the expected stellar positions well within the position accuracy of the SMA data ( $\sim 0''.1$  in an absolute sense, and considerably better in a relative sense for the few cases with multiple disk detections). For stellar components that do not

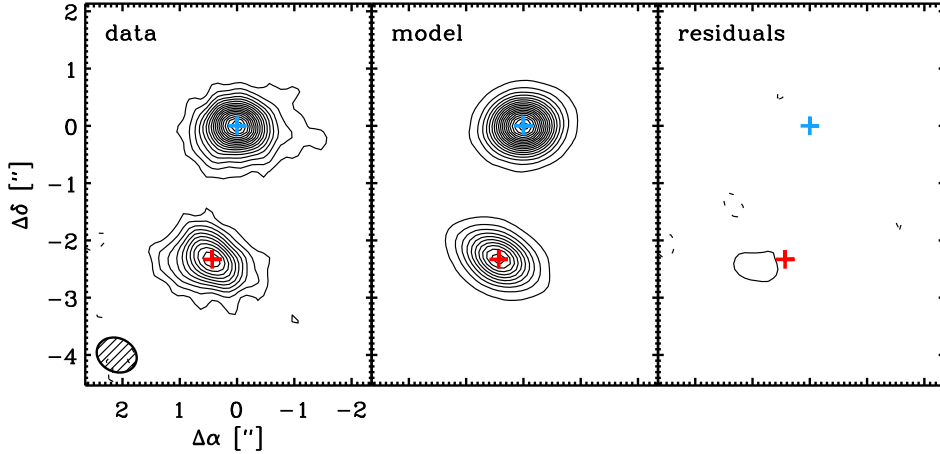


Fig. 5.— Model fit demonstration for the HK Tau binary. From left to right, the panels show the SMA 880  $\mu\text{m}$  image, the best-fit model image, and the imaged residuals. Contours are drawn at  $3\text{mJy beam}^{-1}$  ( $3\sigma$ ) intervals. The synthesized beam is shown in the lower left of the data panel. The HK Tau A and B stellar positions are marked with blue and red crosses, respectively.

exhibit any millimeter emission or may be partially blended with other components, we rely on the positions (or projected angular separations and orientations) provided from optical/infrared measurements in the literature to assign their  $\{\Delta\alpha, \Delta\delta\}$  values. In practice, we estimate the best-fit values of 4 free parameters  $\{F_d, R_d, i_d, \text{PA}_d\}$  and their uncertainties for each resolved disk by comparing model predictions directly with the SMA visibilities using the non-linear  $\chi^2$  minimization routine MPFIT (Markwardt 2009). In each case, several randomized initial parameter sets were employed to avoid trapping in local minima. The results are compiled in Table 4. Figure 5 shows an example model fit for the well-separated and resolved disks of the HK Tau binary.

For 4 of the 14 disks with modeling results in Table 4, the emission is not sufficiently resolved to place meaningful constraints on the disk viewing geometry. In those cases (FX Tau A, UZ Tau Wb, HN Tau A, and Haro 6-37 B), we assumed a fiducial  $\{i_d = 45^\circ, \text{PA}_d = 90^\circ\}$  in order to calculate a reasonable estimate of  $\{F_d, R_d\}$  (alternative viewing geometry selections produce the same flux densities and sizes within the quoted uncertainties). The viewing geometries for the HK Tau B, HV Tau C, and GG Tau Aab disks were fixed based on observations of their scattered light morphologies or molecular kinematics (Duchêne 2010; McCabe et al. 2011; Guilloteau et al. 1999). The UX Tau A and GG Tau Aab disks were modeled as rings, with empty central regions out to radii of 25 and 185 AU based on the more sophisticated analyses of Andrews et al. (2011) and Guilloteau et al. (1999), respectively. The UZ Tau Eab circumbinary disk was also modeled as a ring, with no emission inside a radius of 15 AU: a detailed analysis of this disk will be provided elsewhere (Harris et al., in preparation). Of the remaining 49 individual stars or close-pair composites, 27 have firmly detected – but *unresolved* – millimeter emission and 22 others do not. For simplicity, point source models were used to measure  $F_d$  for the population of detected, but unresolved, disks. After

subtracting models of any emission from nearby stars, upper limits ( $3\sigma$ ) on  $F_d$  were estimated for the undetected components by computing the RMS noise level in a  $4'' \times 4''$  box centered on the stellar position in a synthesized residual map. The point source flux densities and upper limits for these 49 individual stellar components (or close-pair composites) are compiled in Table 5.

The emission from the individual disks in the RW Aur and DD Tau binaries is blended. In these cases, we adopted an iterative modeling strategy. First, a single disk model was fitted to the dominant emission component (the primaries) and subtracted from the data. An initial estimate of the disk model for the blended component (the secondaries) was made from the residuals. Based on those results, a composite model with both disk components was then used to fit the data and derive proper parameter estimates and uncertainties. This method naturally accounts for the blending with inflated formal parameter uncertainties for each model component. None of the disks in these pairs is spatially resolved, so the underlying model for each component disk is a point source.

## 5. Results

We aim to take advantage of this resolved millimeter-wave census to address some key aspects of disk evolution in the presence of stellar companions. To do that, we link our SMA survey results into a comprehensive compilation of stellar separations ( $\rho$ ), component masses ( $M_p$  and  $M_s$ ) and mass ratios ( $q$ ), and millimeter luminosities (defined as the summed emission in a pair:  $F_{\text{pair}} = F_{d,p} + F_{d,s}$ ) for *all* of the known potentially interacting stellar pairs in Taurus (with spectral types F0 to M4). Those data are compiled in Table 6. A complementary list of *single* stars in Taurus with available millimeter-wave observations in the literature is provided in Table 7. We should note that there are 36 other single stars in this spectral type range in the compilation of Luhman et al. (2010) that, to our knowledge, have not yet been observed at millimeter wavelengths.

### 5.1. Millimeter Detection Statistics

If interactions with companions efficiently remove material from circumstellar disks in young multiple systems, there should be a clear signature in the relative detection fractions of millimeter-wave emission (a rough proxy for dust mass) between isolated (single) stars and the individual stellar components of multiple systems: the fraction of stars that exhibit detectable millimeter emission,  $f_{\text{mm}} = N_{\text{det}}/N_{\text{tot}}$ , should be substantially higher for singles compared to multiples. This feature has been noted anecdotally in the past (e.g., Jensen et al. 1994, 1996b; Osterloh & Beckwith 1995; Andrews & Williams 2005), but the inability to assign millimeter emission to individual components in multiple systems has limited any firm quantitative assessment of the detection statistics.

There are millimeter-wave continuum measurements available for 52 single stars in Taurus, 48 binaries (96 stars), 13 triples (39 stars), 7 quadruples (28 stars), 2 quintuples (10 stars), and 1 sextuple (6 stars; the LkH $\alpha$  332 system). Using the component-resolved  $F_d$  measurements in Tables

4 and 5 along with the additional literature photometry compiled in Tables 6 and 7, we computed the  $f_{\text{mm}}$  values for single stars and multiples listed in Table 8. The ranges of  $N_{\text{det}}$  and  $f_{\text{mm}}$  for multiples correspond to the potential distribution of the observed millimeter emission among any unresolved components. We find that 32 of 52 single stars show millimeter emission,  $f_{\text{mm}} = 62 \pm 11\%$ , while only 50-67 of 179 individual stars in multiple systems have millimeter-wave detections,  $f_{\text{mm}} = 28-37 \pm 5\%$ . A two-tailed Fisher Exact test confirms that these are indeed statistically different detection fractions, with a  $p$ -value  $< 0.002$ . Remarkably, the millimeter detection fraction for individual stars in multiple systems does not depend on the number of companions: binaries, triples, and higher-order groups all have  $f_{\text{mm}} \approx 1/3$ , roughly half the detection rate for singles. That uniformity is a testament to the hierarchical nature of multiples, where higher-order ( $N_* \geq 3$ ) systems tend to be constructed of sets of binary pairs.

Given that the detection fraction for stars with companions is roughly half that for stars without them, it may seem natural to assume that only one stellar component in a multiple retains disk material. While not uncommon, this is not necessarily the typical scenario. Of the 48 binaries in Taurus, 20 exhibit millimeter emission. Of those 20 pairs, our millimeter observations have resolved the individual components of 12 (from 24 stars). In 6 of those pairs, the emission is concentrated solely around the primary. In the other 6, both components show some emission – however, the primary is *always* brighter. So, for the sub-population of component-resolved binaries with millimeter emission, the detection fraction for individual stars is actually fairly large (18/24). In the higher order multiples, the situation is slightly more complicated by their hierarchical structure. In some cases, we find dust emission coincident with all components, albeit usually with some pair presumably surrounded by a *circumbinary* disk (e.g., UZ Tau, MHO 1/2). In others, the dust emission is only present around a more isolated, distant companion (e.g., HV Tau, Haro 6-37).

As might be expected, the likelihood that any individual component of a multiple system harbors a circumstellar disk that is massive enough to generate detectable millimeter emission depends critically on the individual details of the system. The following sections explore the potentially observable signatures expected from star-disk interactions, with a more explicit focus on some key connections between the stellar properties tied to orbital dynamics and the basic disk characteristics that can be inferred from the millimeter data.

## 5.2. Pair Demographics and Disk – Star Connections

Theoretical models of star-disk interactions in binary pairs suggest that the separation between the stellar components is the key property that controls the tidal truncation of individual circumstellar disks (Artymowicz & Lubow 1994; Pichardo et al. 2005). These interactions effectively remove mass from the outer regions of these disks (either by accretion or ejection into the local interstellar medium), such that stellar pairs with smaller separations should harbor smaller – and therefore less massive – disks. Since the cool dust in the outer disk that is being stripped by this process emits continuum radiation at millimeter wavelengths, these tidal interactions should

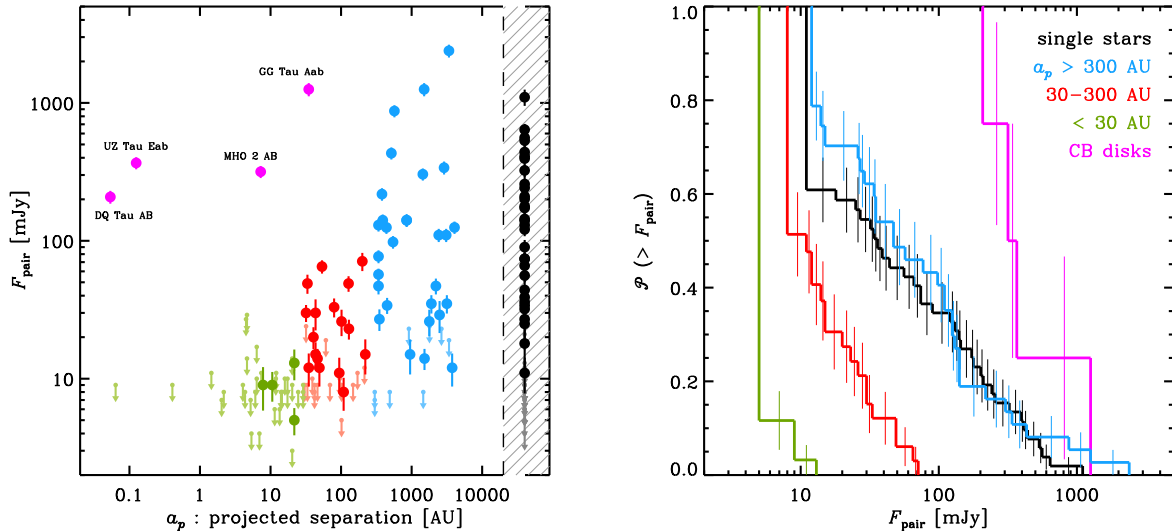


Fig. 6.— (a) A comparison of millimeter flux densities from potentially interacting pairs as a function of the projected pair separation. Single stars are shown to the right of the plot as black points for reference. The pair population can be distinguished into 4 clear sub-categories: wide ( $a_p > 300$  AU), medium ( $a_p = 30\text{--}300$  AU), and small ( $a_p < 30$  AU) pairs, and circumbinary disks (*purple*). (b) The cumulative distributions of millimeter flux densities for each of these sub-categories, constructed with the Kaplan-Meier product-limit estimator to include the available upper limits. Millimeter luminosity is strongly dependent on projected separation.

naturally produce an observable trend where the millimeter luminosity is positively correlated with the separation of the stellar pair. Indeed, the pioneering work on this subject by Jensen et al. (1994, 1996b) clearly identified that the millimeter luminosities for pairs with projected separations  $a_p \leq 50\text{--}100$  AU were statistically lower than their more widely-separated counterparts or single stars. These different populations were confirmed with larger and deeper millimeter-wave surveys (Osterloh & Beckwith 1995; Andrews & Williams 2005), but the detailed distribution of  $F_{\text{pair}}$  with respect to  $a_p$  has remained unclear for two reasons: the low resolution of single-dish millimeter-wave photometry often included several pairs together, and the multiplicity census of the nearest star-forming regions was incomplete. Our survey mitigates these issues, providing an opportunity to look at the details of the millimeter luminosity–separation distribution.

Figure 6a shows  $F_{\text{pair}}$  as a function of  $a_p$  for the 111 stellar pairs in Taurus (see Table 6), along with the 52 single stars that have millimeter-wave measurements (see Table 7; black points, gray upper limits). This diagram is a striking confirmation of the original conclusions of Jensen et al., plainly demonstrating that millimeter continuum luminosities scale with the separation between stellar pairs. However, as the pair separation decreases, the *maximum* millimeter luminosities appear to decline in discrete jumps (rather than continuously) at two relatively well-defined locations:  $a_p \approx 300$  and 30 AU ( $\rho \approx 2$  and  $0.2''$ , respectively). These features facilitate a natural breakdown

of the Taurus pairs into distinct sub-populations. The distribution of  $F_{\text{pair}}$  for wide pairs, with projected separations greater than 300 AU (*blue*), is similar to the distribution for single stars. At medium separations –  $a_p = 30\text{-}300$  AU (*red*) – we find a notable absence of bright pairs and a decreased detection rate. At yet smaller separations,  $a_p < 30$  AU (*green*), only a few pairs exhibit very weak millimeter-wave emission. A small group of dramatic outliers sparsely populate the otherwise empty region of bright pairs with small separations (*purple*): these pairs are known or suspected to harbor massive circumbinary rings (e.g., see Piétu et al. 2011, regarding GG Tau Aab).

The cumulative distributions of  $F_{\text{pair}}$  for each separation-based sub-population can better quantify this apparent trend. The  $\mathcal{P}_a(>F_{\text{pair}})$  distributions shown together in Figure 6b were constructed using the Kaplan-Meier product-limit estimator to properly account for the substantial number of pairs in each sub-population that exhibit no millimeter emission (see Feigelson & Nelson 1985). The distributions are compared directly with the standard two-sample tests used in survival analysis in Table 9. These tests confirm the qualitative examination of Figure 6a: (1) wide pairs and single stars have statistically indistinguishable millimeter luminosity distributions; (2) medium pairs have significantly lower luminosities; and (3) small pairs have yet less millimeter emission. The  $\mathcal{P}_a(>F_{\text{pair}})$  in Figure 6b have similar functional forms, albeit shifted in luminosity. A simple scaling indicates that  $F_{\text{pair}}$  decreases by a factor of  $\sim 5$  from wide to medium separations, and then another factor of 5 from medium to small separations. These trends are not an artifact of including non-detections in the analysis: similar conclusions are drawn by comparing only the detected pairs in the same sub-populations using the two-sided Kolmogorov-Smirnov (K-S) test (see Table 9).

Models of star-disk interactions also postulate an association between the amount of disk truncation and the component masses of the stellar pair. Massive companions impart larger dynamical perturbations to individual disks, producing more tidal stripping, and leading to lower disk masses and therefore less millimeter-wave emission. In that case,  $F_{\text{pair}}$  should be anti-correlated with  $q$ : higher mass ratio pairs should have fainter disk emission. No such trend is obvious in Figure 7a. If we separate the full population into high and low mass ratio pairs at some critical  $q_c$ , we find the largest difference between those sub-categories for  $q_c = 0.5$ . Figure 7b compares the cumulative distributions of the millimeter flux densities for high ( $q > 0.5$ ; *blue*) and low ( $q < 0.5$ ; *red*) mass ratio pairs, again with  $\mathcal{P}_q(> F_{\text{pair}})$  constructed using the Kaplan-Meier estimator to include the pairs that do not have detectable millimeter emission. The same two-sample tests employed above indicate a weak relationship between  $F_{\text{pair}}$  and  $q$  (see Table 9), such that pairs with low stellar mass ratios have slightly less millimeter emission – the opposite of expectations from tidal interaction models. However, the evidence for any increase in the millimeter emission with higher stellar mass ratios is contained entirely in the relative detection ratios: a larger fraction of pairs with low  $q$  are not detected at millimeter wavelengths (see Figure 7a). If only the detected pairs are compared, the millimeter luminosity is found to be independent of  $q$  (see the K-S test results in Table 9). Moreover, this trend is present (and in fact enhanced) only for stellar pairs with wide separations: no clear relationship between  $F_{\text{pair}}$  and  $q$  exists for pairs with  $a_p < 300$  AU (see Table 9).

The absence of a firm connection between the millimeter luminosity and stellar mass ratio for

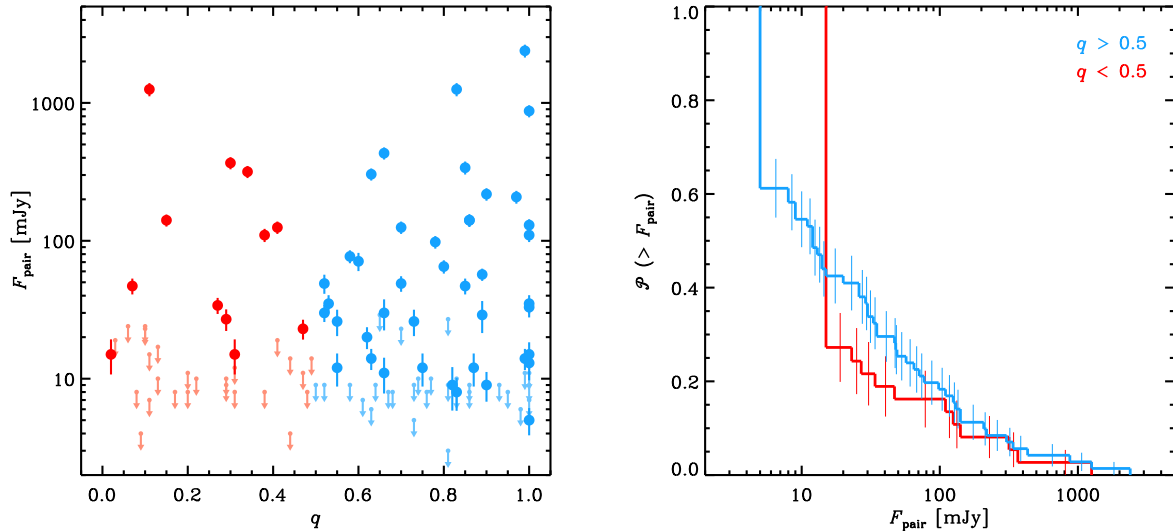


Fig. 7.— (a) A comparison of millimeter flux densities from potentially interacting pairs as a function of stellar mass ratio. For reference, the pair population is distinguished into high ( $q > 0.5$ ; *blue*) and low ( $q < 0.5$ ; *red*) mass ratio groups. (b) The cumulative distributions of millimeter flux densities for high and low mass ratio pairs, constructed with the Kaplan-Meier estimator to include the available upper limits. Millimeter luminosity depends only weakly on the stellar mass ratio.

smaller-separation pairs is consistent with the weak  $q$ -dependence predicted by tidal interaction models. Nevertheless, the correlation between  $F_{\text{pair}}$  and  $q$  for widely-separated pairs is compelling. Since star-disk interactions in these cases should be inherently less destructive, this trend might indicate a relationship between the millimeter luminosity and the absolute (and not relative) stellar masses in the pair. Indeed, Figure 8a demonstrates a marginal association between the millimeter luminosity and total stellar mass in Taurus pairs. Taking only the detections, we find a  $\sim 3\sigma$  correlation between  $F_{\text{pair}}$  and  $M_{\text{pair}}$  (this improves slightly to  $3.7\sigma$  if the labeled outliers are excluded). Figure 8b demonstrates that this relationship is not restricted to stellar pairs, but apparently also applies to *individual* stars, both isolated (single) cases and members of multiple systems. In the latter case, we have combined the component-resolved  $F_d$  estimates from Table 4 and the single star measurements from the literature (Table 7): the result is again a  $\sim 3\sigma$  positive correlation ( $4.5\sigma$  if SU Aur is excluded). It is worth noting that the  $M_*$  distributions for isolated stars and individual stars in multiple systems are statistically indistinguishable. However, it is premature to draw any firm conclusions from these weak trends for two reasons: (1) the dispersion is large relative to the range of the trend, and (2) the stellar masses used here have large systematic uncertainties.

The demographic properties of stellar pairs discussed above are certainly informative, but they also naturally hide some characteristics of individual components that are available from this resolved survey. The two panels in Figure 9 are intended to compare the millimeter-wave luminosities from individual disk components *within* each stellar pair, as a function of their stellar

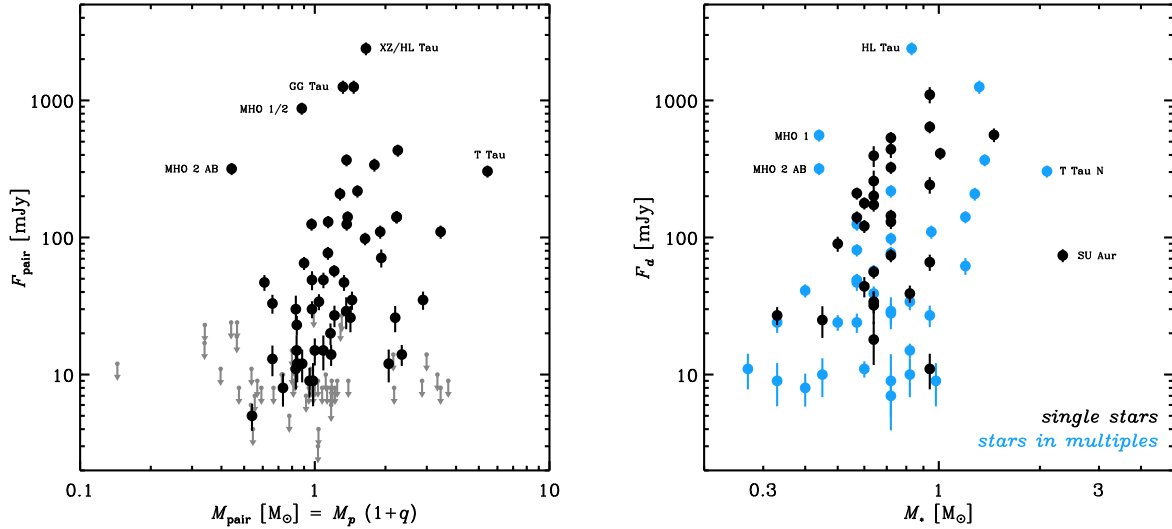


Fig. 8.— (a) Millimeter flux density as a function of the total mass of a stellar pair, where  $M_{\text{pair}} = M_p + M_s = M_p(1 + q)$ . (b) Millimeter flux densities as a function of stellar mass for the individual, detected stellar components in Taurus, for both single stars (*black*) and those in multiple systems (*blue*). Note that upper limits for non-detections are not shown in the right-hand panel.

host masses. Figure 9a directly compares the resolved  $880 \mu\text{m}$  flux densities for each component in each pair. As mentioned in §5.1, the emission from the primary is usually more luminous than from the secondary. The exceptions above the dashed line are comprised of the widely-separated tertiary companions of close pairs and the UZ Tau Wab and FS Tau/Haro 6-5B pairs. The relative dominance of the primary disk emission is unaffected by the projected separation to a companion, and is typically more than would be expected if the amount of millimeter-wave disk emission scales linearly with the stellar host mass. This latter feature is shown more directly in Figure 9b, which compares the cumulative distributions of the ratio of the millimeter flux density to the stellar mass (akin to a disk:star mass ratio) for singles, primaries, and secondaries. In some studies of disks around low-mass stars and brown dwarfs, this  $F_d/M_*$  ratio is found to be roughly constant; the weaker emission (or lower detection rate) is a manifestation of inherently lower host masses (e.g., Scholz et al. 2006; Schaefer et al. 2009). That implicit sensitivity threshold is not the case for the secondaries in our sample: the  $F_d/M_*$  ratio is systematically lower for secondaries compared to primaries and singles, with a probability that it is drawn from the same parent distributions as the primaries or singles of  $<0.008$  (two-sample test results are compiled in Table 9). The results suggest that the millimeter-wave disk emission from the secondaries is inherently less luminous than around the primaries (or isolated stars), regardless of the stellar host mass.



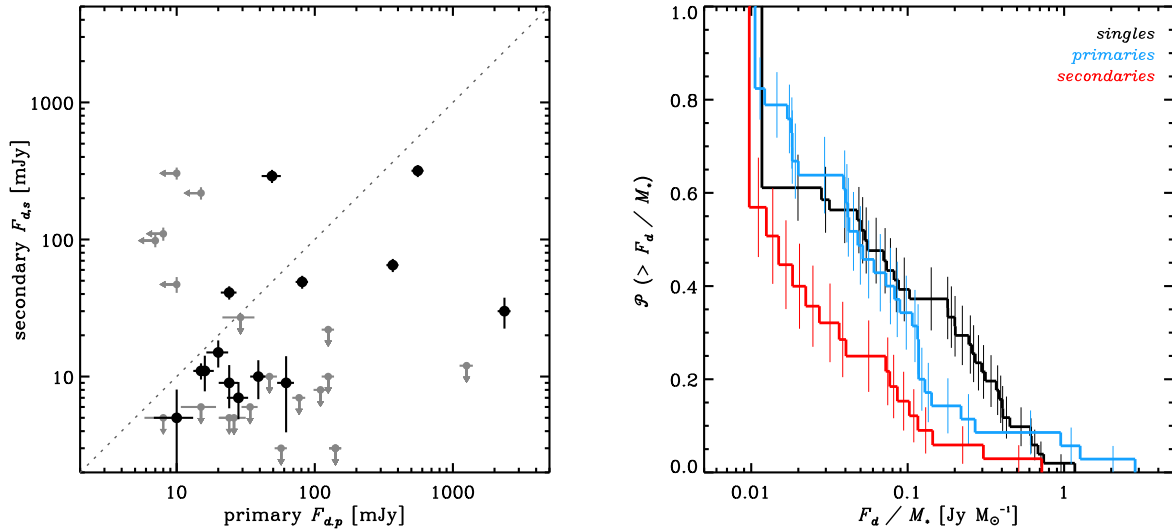


Fig. 9.— (a) The 880  $\mu\text{m}$  flux densities for the primary and secondary components of each stellar pair. (b) The cumulative distributions of the ratio of millimeter-wave disk flux densities to their stellar host masses (a proxy for the disk:star mass ratio) for singles (*black*), primaries (*blue*), and secondaries (*red*), each constructed from the Kaplan-Meier product-limit estimator to include upper limits on  $F_d$ . Two-sample tests (see Table 9) demonstrate that these ratios are systematically lower for secondaries, implying that their disks are inherently less luminous regardless of the host masses.

### 5.3. Disk Sizes and Tidal Truncation

A more direct test of dynamical predictions for star-disk interactions lies with our measurements of individual disk sizes. Theoretical models provide a way to estimate the truncated equilibrium tidal radii ( $R_t$ ) for the disks around each component of a stellar pair given a few key orbital parameters,  $\{a, e, q\}$ , and some characterization of the viscous properties of the disk material (Artymowicz & Lubow 1994). Although they remain uncertain, there are reasonable ways to estimate stellar mass ratios ( $q$ ) from optical/infrared measurements and pre-main sequence stellar evolution models (see the references in Table 6). However, the stellar pairs in this sample have wide enough projected separations that they are expected to have prohibitively long orbital periods and exhibit little apparent motion on reasonable time baselines for observations: therefore, we generally do not have any direct knowledge about their true orbital separations ( $a$ ) or eccentricities ( $e$ ).

Nevertheless, we can construct a probabilistic model of  $R_t$  using only the *projected* physical separation of any pair,  $a_p$  (based on the projected angular separation,  $\rho$ , and assumed distance,  $d$ ). Following Torres (1999), the ratio of the semimajor axis to the projected physical separation is

$$\mathcal{F} \equiv \frac{a}{a_p} = \frac{1 - e^2}{1 + e \cos \nu} \sqrt{1 - \sin^2(\omega + \nu) \sin^2 i}, \quad (1)$$

where  $e$  is the eccentricity,  $\nu$  is the true anomaly,  $\omega$  is the longitude of periastron, and  $i$  is the orbital

inclination relative to the observer (note that the ratio  $\mathcal{F}$  is exact for binaries; we expect only modest deviations from it for well-separated hierarchical pairs). Since we do not know  $\{\omega, i, e, \nu\}$  for any individual stellar pair, we have to construct a probability distribution for the true-to-projected separation ratios,  $\mathcal{P}(\mathcal{F})$ , using a Monte Carlo approach. To accomplish that, we assume that stellar pairs are not observed at any preferential orbital location and adopt uniform distributions for the orbital phase (or mean anomaly) and longitude of periastron ( $\omega$ ). The assumption of random viewing geometries suggests that the distribution of orbital inclinations ( $i$ ) has a  $\sin i$  dependence. However, inferring an appropriate functional form for the eccentricity ( $e$ ) distribution (and by extension the distribution of true anomalies,  $\nu$ ) is more challenging.

There is little empirical information available to constrain the eccentricity distribution for the pre-main sequence binary population. Pairs with short orbital periods have low eccentricities ( $e < 0.1$ ), due to the rapid tidal circularization of their orbits (Zahn 1977; Zahn & Bouchet 1989; Melo et al. 2001). At longer periods, the eccentricity distribution appears relatively uniform in the range  $e \approx 0.1$ -0.9 (Mathieu 1994). It is not clear if the apparent dearth of young stellar pairs with extreme (circular or parabolic) eccentricities is real or an artifact of low-number statistics and selection effects. Based on their samples of main sequence field binaries, Duquennoy & Mayor (1991) and Tokovinin (1998) suggested an increasing eccentricity distribution, where  $\mathcal{P}(e) \propto 2e$  (see also Ambartsumian 1937). However, the recent comprehensive survey of such systems by Raghavan et al. (2010) instead suggests that a flat eccentricity distribution is preferable for orbital periods of  $\sim 10$ - $10^5$  days. Similar results are also noted for very low mass binaries (Dupuy & Liu 2011). Based on these more recent studies, we assume that the eccentricity distribution is uniform. For reference, Figure 10a illustrates the influence of different forms for  $\mathcal{P}(e)$  on the shape of  $\mathcal{P}(\mathcal{F})$ .

Having established the infrastructure to derive a probabilistic model of the true orbital separation ( $a$ ) given the observed projected separation ( $a_p$ ), we can build on that to determine the distribution of tidal truncation radii,  $\mathcal{P}(R_t)$ , for a given stellar pair. Because of its relative simplicity, we adopt the semi-analytic approximations for truncated disk sizes based on the analysis of stable invariant loops by Pichardo et al. (2005). Using their formulation, the tidal radius is

$$R_t \approx 0.337 \left[ \frac{(1-e)^{1.20} \varphi^{2/3} \mu^{0.07}}{0.6 \varphi^{2/3} + \ln(1 + \varphi^{1/3})} \right] \mathcal{F} a_p, \quad (2)$$

where  $\mu = q/(1+q)$  is the mass fraction of the stellar pair and  $\varphi$  is the mass ratio of the host star for which  $R_t$  is being calculated relative to its companion. For example, the truncation radius of the disk around the primary star is calculated with  $\varphi = M_p/M_s = 1/q$ , whereas the  $R_t$  for the disk around the secondary is determined by setting  $\varphi = M_s/M_p = q$ . For any pair in a multiple system, there is a direct measurement of  $a_p$  (or rather  $\rho$ , and an assumed distance) and an estimate of  $q$  (see Table 6). Fixing these quantities, we constructed the probability distribution  $\mathcal{P}(R_t)$  that a component of the pair hosts a disk with a tidally truncated radius  $R_t$  using a Monte Carlo simulation with  $\sim 10^7$  realizations of Equation (2), assuming the priors for the distributions of the orbital elements  $\{\omega, i, e, \nu\}$  (and therefore  $\mathcal{F}$ ) discussed above.

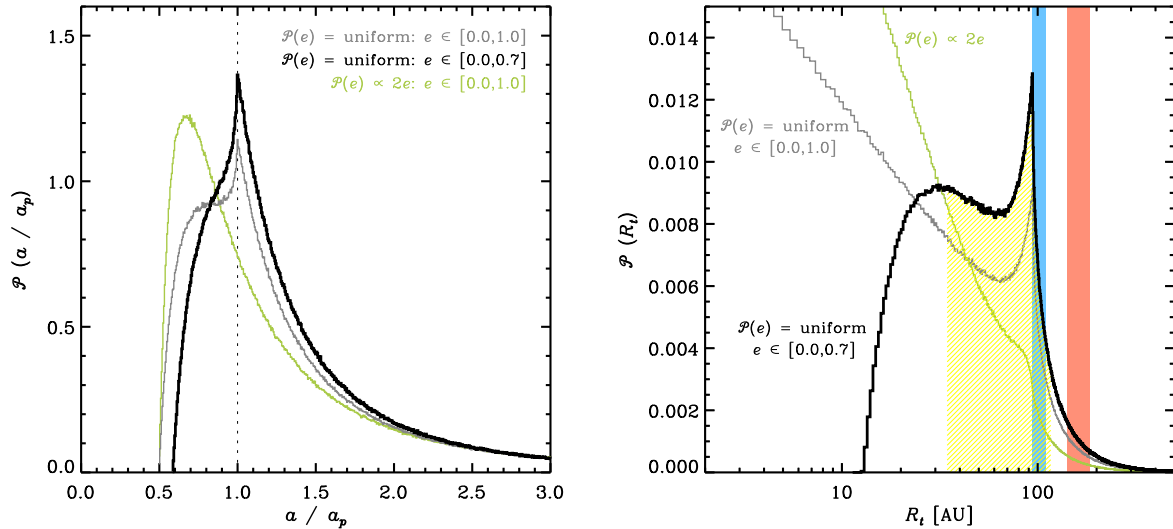


Fig. 10.— (a) Probability distributions for the ratio of true to projected separations,  $\mathcal{P}(\mathcal{F})$  where  $\mathcal{F} \equiv a/a_p$ , using three different underlying eccentricity distributions. (b) An example probability distribution for the disk radii ( $R_t$ ) expected in the HK Tau binary based on the tidal interaction models of Pichardo et al. (2005) for the same three assumed eccentricity distributions. The blue and red vertical bars represent the best-fit disk radii (and  $1\sigma$  uncertainties) for HK Tau A and B, respectively, measured directly from the SMA visibilities in §4. The yellow filled area marks the region containing 68% of the probability for the  $\mathcal{P}(R_t)$  with the favored eccentricity distribution (black curve; see text), used to determine the error bars in Figure 11.

As an example, Figure 10b shows  $\mathcal{P}(R_t)$  for the HK Tau binary, where  $a_p = 340$  AU and  $q \approx 1$ , for three representative assumptions about the underlying eccentricity distribution (note that the same  $R_t$  distribution applies to both components for this equal-mass stellar pair). The best-fit estimates of the disk radii from our modeling of the SMA data (see §4) are marked as red (HK Tau A) and blue (HK Tau B) vertical bars. Tidal interaction models predict that the disk sizes have a rather steep dependence on the orbital eccentricity (see Equation 2), which means that the assumption of an underlying  $\mathcal{P}(e)$  that permits or favors high eccentricities will lead to the *general* prediction of very small disk sizes (gray or green curves in Figure 10b) and, therefore, low millimeter-wave luminosities. While such eccentricity distributions may be relevant for the general population of multiple systems, the luminosity-based selection criterion used to build our component-resolved SMA sample creates a strong bias that would exclude high- $e$  pairs. With that bias in mind, we favor the use of a truncated eccentricity distribution to make comparisons between the measured and predicted disk radii; we assume  $\mathcal{P}(e)$  is uniform for  $e \in [0.0, 0.7]$  (black curves in Figure 10).

Figure 11 makes a direct comparison between the measurements of dust disk sizes ( $R_d$ ) that were determined in §4 (see Tables 4 and 5) and the truncation radii ( $R_t$ ) predicted by our probabilistic treatment of the Pichardo et al. (2005) models. The location of the points along the  $R_t$

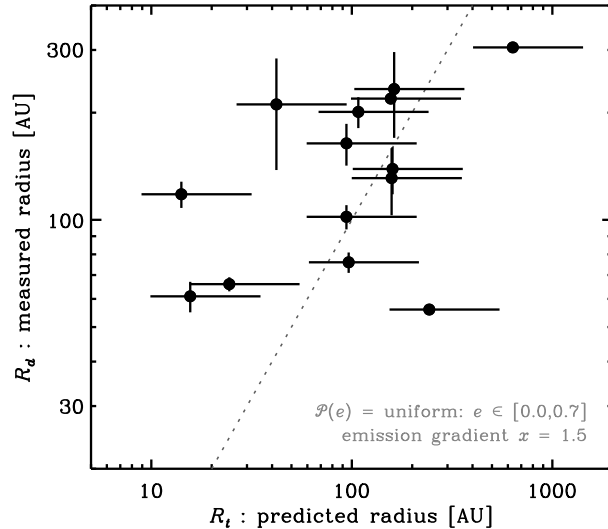


Fig. 11.— The measured disk radii (see Tables 4 and 5) compared with the expected disk radii based on a probabilistic treatment of the Pichardo et al. (2005) tidal interaction models, for an assumed underlying uniform eccentricity distribution truncated at  $e = 0.7$  (see text).

axis (abscissae) correspond to the peaks of their  $\mathcal{P}(R_t)$  distributions (for the assumed  $\mathcal{P}(e)$  described above), and their asymmetric error bars encapsulate the central 68% of those probability distributions (see the shaded yellow region of Figure 10b for an example). Of the 14 disks with available  $R_d$  measurements, eight have sizes that are in good agreement with predictions from the tidal interaction models, two are smaller than expected (around GG Tau Aab and DK Tau A), and the remaining four are considerably larger. These decidedly mixed results for the Pichardo et al. (2005) model predictions could be at least partially ameliorated by introducing a term that incorporates viscosity into the interaction calculations, which would tend to increase  $R_t$  due to the viscous spreading of disk material (see Artymowicz & Lubow 1994). Quantitatively comparable shifts in the measured  $R_d$  values could be accommodated by permitting a range of emission gradients ( $x$ ) in model fits to the observations. Reconciling the measured disk sizes with the predictions from tidal interaction models would require that the disk viscosity increases and/or the millimeter-wave emission gradient ( $x$ ) decreases as a function of pair separation ( $a$ ).

## 6. Discussion

We have carried out a luminosity and separation limited survey of the millimeter-wave dust continuum emission from the disks around individual components of 23 young multiple star systems in the  $\sim 1$ -2 Myr-old Taurus-Auriga star formation region. With a simple morphological model, we fitted the continuum visibilities observed with the SMA interferometer to determine the luminosity and size of each individual disk in these systems. These component-resolved measurements were

then coupled with a comprehensive database of millimeter-wave luminosities for *all* of the multiple systems in Taurus (with spectral types F0-M4) to estimate millimeter detection frequencies, evaluate the dependence of continuum emission levels on the separations and masses of companion stars, and make direct comparisons with predictions from tidal interaction models.

We find that roughly one third (28-37%) of the individual stars in multiple systems harbor disks with dust masses that are large enough to emit detectable millimeter continuum radiation (see §5.1). This low incidence rate is approximately half that for isolated single stars (62%), and does not depend on the number of stellar companions in the system. Similar disk frequencies have been inferred from accretion and infrared excess signatures (Cieza et al. 2009; Kraus et al. 2012), although without component-resolved diagnostics. Given these disk frequencies, it is clear that some *external* processes driven by the presence of a companion act to hasten the dispersal of circumstellar material in multiple systems at a level comparable to any *internal* disk evolution mechanisms (e.g., photoevaporation, grain growth, planet formation, etc.) on  $\sim 1$ -2 Myr timescales.

Some basic demographic properties of stellar pairs in Taurus can provide new insights into the mechanics of those external evolution processes. Building on the initial work by Jensen et al. (1994, 1996b), we have shown that the millimeter-wave luminosity from a pair of stars depends strongly on their (projected) separation (see §5.2). We identified substantial changes in the millimeter luminosity distributions of pair populations at discrete separations of 30 and 300 AU. Widely-separated pairs ( $a_p > 300$  AU) have emission levels similar to single stars. Pairs with medium separations ( $a_p = 30$ -300 AU) are typically  $5\times$  fainter, with a lower overall detection fraction. Millimeter emission is rarely detected around pairs with small separations ( $a_p < 30$  AU), representing at least another factor of  $\sim 5$  reduction in luminosity. We demonstrated that there is a weak tendency for pairs with comparable stellar masses (higher  $q$ ) to have brighter millimeter emission, with the effect being considerably stronger for wider pairs. We suggested this is related to a marginal correlation between stellar mass and millimeter luminosity, although verifying that tentative trend is a challenge due to the systematic uncertainties involved in estimating stellar masses.

The relationship between millimeter luminosity and pair separation (Fig. 6) suggests that the external process relevant for the evolution of circumstellar material in multiple systems may be tied to tidal stripping from the outer regions of their constituent disks (e.g., Artymowicz & Lubow 1994). However, we found mixed results in a comparison of individual disk sizes that were measured (from the SMA data; §4) and predicted from tidal interaction models (see §5.3). Using a probabilistic treatment of orbital parameters, we showed that about half of the resolved disks in our sample have sizes that are consistent with the truncation predictions of the Pichardo et al. (2005) models. Most of the remainder have sizes that are substantially larger than expected, given the smaller projected separations to their companions (Fig. 11). Analogous discrepancies have been noted regarding the observed and predicted inner edges of circumbinary rings (e.g., Beust & Dutrey 2005; Nagel et al. 2010). These results hint that *another* external process also shapes the circumstellar environments of young multiples. Further support for this additional evolutionary process is found in the observed distributions of circumstellar dust around individual stellar components. Tidal interaction models

predict that disks should survive around both components of a pair, with their relative sizes roughly set by  $q$  (for a given  $a$ ). However, Fig. 9 (see §5.2) demonstrates that this is often not the case. Roughly half of the multiple systems with detectable millimeter emission harbor only a single disk, usually around the primary component (or the wide tertiary in some hierarchical triples; e.g., HV Tau or Haro 6-37). Moreover, aside from a few exceptional counterexamples (see Fig. 6a), we find little millimeter-wave evidence for the circumbinary disks that should be common around pairs with small separations if tidal interactions were the sole external evolution mechanism.

To be fair, tidal interactions alone may still be able to explain many of these observed properties. The processes of stripping and truncation in pairs where the orbital and disk planes are misaligned has not yet been explored in detail (although see, e.g., Akeson et al. 2007; Verrier & Evans 2008), but might be substantially enhanced for some configurations. With limited orbital information, the prevalence of such misalignment is not known: but, there is some indication from polarization measurements that it is common (Jensen et al. 2004) and a number of specific examples have been identified (e.g., HK Tau or HD 98800; Duchêne et al. 2003; Andrews et al. 2010). Moreover, it is important to keep in mind that the emission we have measured is only capable of probing the trace population of dust particles in these disks, and not their dominant mass reservoirs of molecular gas. The total disk masses that would be inferred from this emission could be substantially under-estimated (see Andrews & Williams 2005, 2007a), as could the apparent disk sizes (e.g., Hughes et al. 2008; Panić et al. 2009; Andrews et al. 2012). Future complementary observations of emission line probes would help better address such uncertainties.

Alternatively, the disk properties we observe may be set at very early stages by the processes that regulate accretion during multiple star formation. Numerical simulations indicate that the ratio of the specific angular momenta of the infalling material ( $j_{\text{gas}}$ ) to the stellar pair ( $j_*$ ) is fundamental in determining how the gas and dust accreted from a proto-system envelope is distributed among individual stellar components (Bonnell & Bate 1994; Bate & Bonnell 1997). If  $j_{\text{gas}} < j_*$ , most of the infalling material will form a disk around the stellar primary. Conversely, if  $j_{\text{gas}} \geq j_*$ , then a circum-secondary or circumbinary disk will dominate (see also Ochi et al. 2005). In the many cases with only circum-primary disk detections described above, the data are consistent with the former scenario. Similar millimeter-wave observations suggest that primary stars preferentially harbor more circumstellar material at the even earlier Class 0/I stages of protostellar evolution (e.g., Launhardt 2004; Patience et al. 2008, and references therein).

To summarize, there is a body of observational evidence suggesting that (at least) two fundamental processes related to the presence of stellar companions play significant roles in the evolution of circumstellar material in young multiple systems. The first is associated with the multiple star formation process itself, where the fraction of angular momentum associated with infalling material relative to that contained in the orbital motion of the stellar pair determines how circumstellar material is apportioned to each component. This is likely responsible for the pairs we observe with very large primary-to-secondary millimeter luminosity ratios. The second is a tidal interaction process that strips material from any individual disks that survive the formation process. This is

thought to be the origin of the millimeter luminosity – pair separation relationship.

At the typical  $\sim 1\text{-}2$  Myr age of Taurus-Auriga multiples, both of these evolution mechanisms have already made their mark on disk properties. The long-term fate of the circumstellar material in these multiple systems now rests with the same internal mechanisms that govern the subsequent evolution and dissipation of the disks around their isolated (single) counterparts. The formation and evolution of planets from this disk material are mechanisms of particular interest in these systems. The relatively straightforward, albeit uncertain, relationship between millimeter-wave luminosities and total disk masses enables at least a preliminary assessment of the likelihood of planet formation around individual components in multiple systems. Using the conversion advocated by Andrews & Williams (2005, 2007a) – which assumes optically thin, isothermal dust emission with a mean temperature of 20 K and (gas+dust) opacity of  $0.034 \text{ cm}^2 \text{ g}^{-1}$  at  $880 \mu\text{m}$  –  $F_d \approx 15 \text{ mJy}$  corresponds to a disk mass of  $\sim 1 M_{\text{Jup}}$ , and  $F_d \approx 150 \text{ mJy}$  represents the standard estimate of the minimum mass of the solar nebula,  $\sim 0.01 M_{\odot}$ . Taking these conversions at face value, we would conclude that giant planets are unlikely to form around stars in close pairs (Fig. 6) or around the secondary components of most pairs with wider separations (Fig. 9). However, we would likewise infer that the primary components in wider pairs, the wide tertiaries in hierarchical triples, and perhaps the population of spectroscopic binaries should be just as likely to host giant planets as single stars.

Direct exoplanet searches of main sequence multiple systems in the field confirm these general expectations from the disk survey: planet formation is not severely inhibited by the presence of a stellar companion (e.g., Patience et al. 2002; Raghavan et al. 2006; Duchêne 2010), and giant planets are preferentially found around primaries, the isolated components of hierarchical triples (Desidera & Barbieri 2007; Bonavita & Desidera 2007; Mugrauer & Neuhäuser 2009; Desidera et al. 2011), and perhaps even spectroscopic binaries (e.g., Doyle et al. 2011). That corroboration of results is a promising sign for planet formation studies in multiple systems, but the characterization of the disks around individual stellar components in these systems is still in its early stages. In the near future, we expect that new facilities like the Atacama Large Millimeter Array (ALMA) will shift the focus to study these individual disks in detail to directly compare their density structures and particle growth signatures with the disks around isolated (single) stars. Ultimately, such observations will help determine the impact of a nearby stellar neighbor on the planet formation process.

## 7. Summary

We have presented the results of an SMA imaging survey of the millimeter-wave ( $880 \mu\text{m}$  or  $1.3 \text{ mm}$ ) thermal continuum emission from circumstellar dust in 23 young multiple systems in the Taurus-Auriga star-forming region. This census was designed to target relatively bright ( $>20 \text{ mJy}$  at  $880 \mu\text{m}$ ) and well-separated ( $\rho > 0''.3$ ) systems with primary spectral types between F0 and M4. We employed simple morphological models of the SMA visibilities to measure component-resolved

millimeter luminosities and disk sizes whenever possible. Those results were considered together with a comprehensive literature compilation of the millimeter luminosities from *all* Taurus multiples (in this spectral type range) to better analyze how the presence of a stellar companion affects basic disk properties. Our primary conclusions are the following:

1. The millimeter detection frequency for individual stars in multiple systems is approximately 1/3 (28-40%), about half that for single stars (62%), and independent of the number of companions. These relative incidence rates suggest that the presence of a stellar companion plays a substantial *external* role in the early development and evolution of circumstellar material, at a level comparable to the standard *internal* disk evolution mechanisms that can operate in isolation (e.g., photoevaporation, particle growth, planet formation, etc.).
2. The millimeter luminosity from a pair of stars depends strongly on their projected separation ( $a_p$ ), such that closer pairs are substantially fainter. We find natural breaks in the luminosity–separation plane at  $a_p \approx 30$  and 300 AU. The luminosity distribution of wide pairs ( $a_p > 300$  AU) is indistinguishable from that of single stars. Pairs with medium separations ( $a_p = 30$ -300 AU) are  $5\times$  fainter, and the very few close pairs ( $a_p < 30$  AU) that we detect are  $5\times$  fainter yet – although a few bright *circumbinary* disks represent notable exceptions.
3. There is no clear relationship between the millimeter luminosity from a pair and its stellar mass ratio ( $q$ ) in general, but wide pairs with higher  $q$  tend to be brighter. We show that this latter behavior is produced by a marginal correlation between millimeter luminosities and stellar masses (both summed among pairs and for individual stars). However, the significance of this trend is questionable: the scatter is large, and there are substantial systematic uncertainties in estimating individual stellar masses that are not considered here. In nearly all cases, the primary component of a binary pair or the wide tertiary of a hierarchical triple harbors the disk material that dominates the millimeter luminosity of the system (higher-order systems show a range of behavior, depending on the hierarchical nature of their pairings).
4. We find mixed results from a direct comparison of the disk sizes measured from the data and predicted from tidal interaction models, based on a probabilistic treatment of the orbital parameters for each system. Of the 15 resolved disks in our sample, the radii expected from the models described by Pichardo et al. (2005) are commensurate with the observed radii for eight disks; two others are found to be too small, and the remaining five are notably larger than would be expected given the relatively small (projected) distances to their companions.
5. These millimeter-wave observations suggest that at least two external mechanisms contribute to the evolution of circumstellar material in young multiple star systems. Star-disk tidal interactions strip material from the outer regions of individual disks, a process responsible for the strong dependence of the millimeter luminosity on the projected separation to a companion. We are lead to infer that accretion during the multiple star formation process itself also plays a substantial role in apportioning disk material, in many cases setting the



initial disk masses such that primary stars harbor substantially more circumstellar material than their companions. The long-term prospects for (giant) planet formation in multiple systems are poor for stars in close pairings and around secondaries, but should be comparable to those around single stars for primaries, wide tertiaries in hierarchical triples, and perhaps around both components of very close spectroscopic binaries.

We are grateful to Trent Dupuy for his assistance with the probabilistic treatment of projected orbits, to Joanna Brown for kindly providing some supplementary observing time on the FQ Tau binary, and to an anonymous referee for helpful suggestions on clarifying the draft manuscript. The Submillimeter Array (SMA) is a joint project between the Smithsonian Astrophysical Observatory and the Academia Sinica Institute of Astronomy and Astrophysics and is funded by the Smithsonian Institution and the Academia Sinica.

Table 1. Selected Sample of Taurus Multiples

| System                  | $N_*$ | $N_{\text{pair}}$ |
|-------------------------|-------|-------------------|
| MHO 1/MHO 2             | 3     | 2                 |
| DD Tau                  | 2     | 1                 |
| FQ Tau                  | 2     | 1                 |
| T Tau                   | 3     | 2                 |
| <i>FS Tau/Haro 6-5B</i> | 3     | 2                 |
| FV Tau                  | 4     | 3                 |
| DI Tau/DH Tau           | 4     | 3                 |
| UX Tau                  | 4     | 4                 |
| FX Tau                  | 2     | 1                 |
| DK Tau                  | 2     | 1                 |
| <i>XZ Tau/HL Tau</i>    | 3     | 2                 |
| HK Tau                  | 2     | 1                 |
| V710 Tau                | 3     | 2                 |
| GG Tau                  | 4     | 3                 |
| <i>FZ Tau/FY Tau</i>    | 2     | 1                 |
| UZ Tau                  | 4     | 3                 |
| JH 112                  | 3     | 2                 |
| <i>V807 Tau/GH Tau</i>  | 5     | 4                 |
| GI Tau/GK Tau           | 2     | 1                 |
| HN Tau                  | 2     | 1                 |
| IT Tau                  | 2     | 1                 |
| HP Tau                  | 4     | 4                 |
| HV Tau                  | 3     | 2                 |
| Haro 6-37               | 3     | 2                 |
| UY Aur                  | 2     | 1                 |
| CIDA-9                  | 2     | 1                 |
| RW Aur                  | 2     | 1                 |

Note. — Col. (1): System name. Italicized systems have not been re-observed with the SMA (see §2). Col (2): Number of stars in system. Col. (3): Number of “pairs” in system (see §2).

Table 2. SMA Observing Log

| UT Date     | Targets  | Config. | $\nu(\text{LO})$<br>[GHz] |
|-------------|--|---------|---------------------------|
| 2005 Dec 17 | DH/DI Tau  | C       | 340.755                   |
| 2009 Oct 24 | DK Tau   | C       | 340.767                   |
| 2010 Feb 11 | DK Tau   | V       | 343.277                   |
| 2010 Feb 18 | UZ Tau   | V       | 341.536                   |
| 2010 Feb 19 | HK Tau   | V       | 342.289                   |
| 2010 Mar 2  | UZ Tau   | V       | 340.427                   |
| 2010 Nov 10 | IT Tau, FX Tau, HK Tau,<br>V710 Tau, HN Tau, CIDA-9            | C       | 340.755                   |
| 2010 Nov 11 | FQ Tau, IT Tau, FV Tau,<br>HV Tau, JH 112                      | C       | 340.755                   |
| 2010 Nov 12 | FQ Tau, IT Tau, FV Tau,<br>HV Tau, JH 112                      | C       | 340.755                   |
| 2010 Dec 13 | RW Aur, Haro 6-37, DD Tau,<br>T Tau, UY Aur                    | C       | 340.755                   |
| 2010 Dec 25 | HP Tau   | C       | 225.497                   |
| 2010 Dec 27 | GG Tau, GI/GK Tau, MHO 1/2                                     | C       | 225.497                   |
| 2011 Jan 28 | FQ Tau   | E       | 340.755                   |
| 2011 Feb 3  | FV Tau, FX Tau, T Tau  | E       | 340.755                   |
| 2011 Feb 17 | UZ Tau, UY Aur, DD Tau   | E       | 340.755                   |
| 2011 Aug 16 | DD Tau   | E       | 341.575                   |
| 2012 Jan 24 | FV Tau, FX Tau, UY Aur   | E       | 340.755                   |
| 2011 Oct 13 | J04080782+2807280, MHO 3<br>J04141188+2811535, V410 X-ray 7    | C       | 225.497                   |
| 2011 Oct 27 | V710 Tau C, J04414565+2301580<br>J04554757+3028077, CFHT Tau 7 | C       | 222.709                   |

Note. — Col. (1): UT date of observations. Col. (2): Multiple systems observed. Col. (3): SMA antenna configuration (see §3). Col. (4): LO frequency setting. Note that the observations below the horizontal line focused on multiple systems that are *not* part of our sample: they were observed because there were no previous millimeter-wave measurements of these systems available in the literature (see §5.1).

Table 3. Properties of Synthesized Continuum Maps

| System    | $\lambda$                | RMS noise                  | beam size        | beam PA             |
|-----------|--------------------------|----------------------------|------------------|---------------------|
| (1)       | [ $\mu\text{m}$ ]<br>(2) | [mJy beam $^{-1}$ ]<br>(3) | [ $''$ ]<br>(4)  | [ $^\circ$ ]<br>(5) |
| MHO 1/2   | 1335                     | 2.1                        | $2.8 \times 2.2$ | 95                  |
| DD Tau    | 880                      | 1.9                        | $0.9 \times 0.7$ | 79                  |
| FQ Tau    | 880                      | 1.2                        | $0.9 \times 0.7$ | 77                  |
| T Tau     | 880                      | 3.6                        | $1.0 \times 0.8$ | 77                  |
| FV Tau    | 880                      | 1.1                        | $1.0 \times 0.7$ | 79                  |
| DI/DH Tau | 880                      | 3.3                        | $2.6 \times 2.1$ | 151                 |
| UX Tau    | 880                      | 0.9                        | $0.6 \times 0.4$ | 33                  |
| FX Tau    | 880                      | 1.6                        | $1.1 \times 0.8$ | 82                  |
| DK Tau    | 880                      | 0.7                        | $0.5 \times 0.5$ | 0                   |
| HK Tau    | 880                      | 1.4                        | $0.7 \times 0.6$ | 65                  |
| V710 Tau  | 880                      | 3.2                        | $2.2 \times 2.0$ | 94                  |
| GG Tau    | 1335                     | 2.2                        | $3.2 \times 2.4$ | 32                  |
| UZ Tau    | 880                      | 0.7                        | $0.4 \times 0.3$ | 51                  |
| JH 112    | 880                      | 1.9                        | $2.0 \times 1.8$ | 57                  |
| GI/GK Tau | 1335                     | 0.7                        | $3.6 \times 2.6$ | 68                  |
| HN Tau    | 880                      | 2.1                        | $2.2 \times 2.0$ | 96                  |
| IT Tau    | 880                      | 1.4                        | $2.1 \times 1.9$ | 78                  |
| HP Tau    | 1335                     | 1.2                        | $3.9 \times 2.9$ | 102                 |
| HV Tau    | 880                      | 2.3                        | $2.0 \times 1.8$ | 61                  |
| Haro 6-37 | 880                      | 5.0                        | $2.1 \times 2.0$ | 136                 |
| UY Aur    | 880                      | 1.5                        | $0.9 \times 0.6$ | 91                  |
| CIDA-9    | 880                      | 2.4                        | $2.2 \times 2.0$ | 98                  |
| RW Aur    | 880                      | 3.6                        | $2.1 \times 2.0$ | 159                 |

Note. — Col. (1): System name. Col. (2): Effective observing wavelength. Col. (3): RMS noise level ( $1\sigma$ ) in the naturally weighted synthesis image (see Figures 2-4). Col. (4) & (5): Beam dimensions and major axis position angle.

Table 4. Resolved Disk Properties

| Name        | Disk Center      |                  | $F_d$<br>[mJy] | $R_d$<br>[AU] | $i_d$<br>[°] | $PA_d$<br>[°] |
|-------------|------------------|------------------|----------------|---------------|--------------|---------------|
|             | $\alpha$ [J2000] | $\delta$ [J2000] |                |               |              |               |
| (1)         | (2)              | (3)              | (4)            | (5)           | (6)          | (7)           |
| MHO 1       | 04 14 26.28      | +28 06 02.90     | (242 ± 3)      | 131 ± 28      | 32 ± 15      | 84 ± 28       |
| T Tau N     | 04 21 59.44      | +19 32 06.31     | 304 ± 3        | 64 ± 3        | 6 ± 21       | 90 ± 36       |
| UX Tau A    | 04 30 04.00      | +18 13 49.25     | 141 ± 1        | 57 ± 1        | 34 ± 2       | 174 ± 4       |
| FX Tau A    | 04 30 29.64      | +24 26 44.77     | 24 ± 3         | 219 ± 57      | [45]         | [90]          |
| DK Tau A    | 04 30 44.25      | +26 01 24.52     | 57 ± 1         | 76 ± 5        | 27 ± 9       | 115 ± 12      |
| HK Tau A    | 04 31 50.57      | +24 24 17.60     | 81 ± 2         | 102 ± 8       | 57 ± 4       | 118 ± 5       |
| HK Tau B    | 04 31 50.60      | +24 24 15.27     | 49 ± 2         | 164 ± 22      | [84]         | [40]          |
| GG Tau Aab  | 04 32 30.36      | +17 31 40.03     | (557 ± 3)      | 305 ± 5       | [37]         | [7]           |
| UZ Tau Eab  | 04 32 43.07      | +25 52 30.80     | 367 ± 3        | 219 ± 3       | 50 ± 1       | 86 ± 1        |
| UZ Tau Wa   | 04 32 42.83      | +25 52 31.04     | 24 ± 2         | 63 ± 6        | 56 ± 4       | 40 ± 6        |
| UZ Tau Wb   | 04 32 42.83      | +25 52 31.41     | 41 ± 2         | 119 ± 10      | [45]         | [90]          |
| HN Tau A    | 04 33 39.38      | +17 51 52.12     | 34 ± 3         | 233 ± 63      | [45]         | [90]          |
| HV Tau C    | 04 38 35.47      | +26 10 41.24     | 98 ± 3         | 139 ± 21      | [80]         | 99 ± 9        |
| Haro 6-37 B | 04 46 59.09      | +17 02 39.87     | 218 ± 6        | 219 ± 15      | [45]         | [90]          |

Note. — Col. (1): Stellar component name. Col. (2) and (3): Adopted disk center coordinates. Col. (4): Flux density. Values in parenthesis correspond to measurements at a wavelength of 1.3 mm: all others are at 880  $\mu$ m. Col. (5): Disk radius. Col. (6): Disk inclination angle, where 0° is face-on. Col. (7): Position angle (E of N) of the disk major axis projected on the sky. Values in square brackets were fixed in the modeling (see §4).

Table 5. Unresolved Disk Properties

| Name             | Disk Center      |                  | $F_d$<br>[mJy] | Name               | Disk Center      |                  | $F_d$<br>[mJy] |
|------------------|------------------|------------------|----------------|--------------------|------------------|------------------|----------------|
|                  | $\alpha$ [J2000] | $\delta$ [J2000] |                |                    | $\alpha$ [J2000] | $\delta$ [J2000] |                |
| MHO 2 AB         | 04 14 26.47      | +28 05 59.95     | $(138 \pm 1)$  | GG Tau Bb          | 04 32 30.51      | +17 31 28.68     | $(< 7)$        |
| DD Tau A         | 04 18 31.13      | +28 16 28.82     | $24 \pm 3$     | <i>FZ Tau</i>      | 04 32 31.76      | +24 20 03.10     | $29 \pm 7$     |
| DD Tau B         | 04 18 31.13      | +28 16 28.26     | $9 \pm 3$      | <i>FY Tau</i>      | 04 32 30.58      | +24 19 57.29     | $< 27$         |
| FQ Tau A         | 04 19 12.81      | +28 29 32.75     | $8 \pm 2$      | JH 112 Aa          | 04 32 49.12      | +22 53 02.52     | $10 \pm 3$     |
| FQ Tau B         | 04 19 12.79      | +28 29 33.44     | $< 5$          | JH 112 Ab          | 04 32 49.22      | +22 53 03.04     | $5 \pm 3$      |
| T Tau Sab        | 04 21 59.44      | +19 32 05.61     | $< 10$         | JH 112 B           | 04 32 49.27      | +22 53 07.89     | $< 6$          |
| <i>FS Tau AB</i> | 04 22 02.18      | +26 57 30.49     | $49 \pm 6$     | <i>V807 Tau AB</i> | 04 33 06.64      | +24 09 54.90     | $20 \pm 3$     |
| <i>Haro 6-5B</i> | 04 22 00.70      | +26 57 32.50     | $(134 \pm 6)$  | <i>GH Tau AB</i>   | 04 33 06.22      | +24 09 33.99     | $15 \pm 3$     |
| FV Tau A         | 04 26 53.53      | +26 06 54.10     | $15 \pm 1$     | GK Tau             | 04 33 34.57      | +24 21 05.64     | $(3 \pm 1)$    |
| FV Tau B         | 04 26 53.47      | +26 06 54.12     | $11 \pm 1$     | GI Tau             | 04 33 34.06      | +24 21 16.83     | $(12 \pm 1)$   |
| FV Tau/c A       | 04 26 54.41      | +26 06 50.77     | $< 5$          | HN Tau B           | 04 33 39.24      | +17 51 49.71     | $< 6$          |
| FV Tau/c B       | 04 26 54.36      | +26 06 51.03     | $< 5$          | IT Tau A           | 04 33 54.71      | +26 13 27.36     | $16 \pm 2$     |
| DI Tau AB        | 04 29 42.46      | +26 32 49.38     | $< 10$         | IT Tau B           | 04 33 54.59      | +26 13 25.21     | $11 \pm 3$     |
| DH Tau A         | 04 29 41.64      | +26 32 58.34     | $47 \pm 4$     | HP Tau/G3 AB       | 04 35 53.50      | +22 54 09.84     | $(< 4)$        |
| DH Tau B         | 04 29 41.74      | +26 32 56.56     | $< 10$         | HP Tau/G2          | 04 35 54.16      | +22 54 13.48     | $(< 4)$        |
| UX Tau Bab       | 04 30 03.59      | +18 13 49.18     | $< 3$          | HP Tau             | 04 35 52.77      | +22 54 23.17     | $(48 \pm 2)$   |
| UX Tau C         | 04 30 04.00      | +18 13 43.39     | $< 3$          | HV Tau AB          | 04 38 35.29      | +26 10 38.16     | $< 7$          |
| FX Tau B         | 04 30 29.58      | +24 26 45.06     | $< 5$          | Haro 6-37 Aab      | 04 46 58.98      | +17 02 37.90     | $< 15$         |
| DK Tau B         | 04 30 44.39      | +26 01 23.45     | $< 3$          | UY Aur A           | 04 51 47.39      | +30 47 13.31     | $39 \pm 3$     |
| <i>XZ Tau AB</i> | 04 31 40.07      | +18 13 57.18     | $(14 \pm 3)$   | UY Aur B           | 04 51 47.34      | +30 47 12.71     | $10 \pm 3$     |
| <i>HL Tau</i>    | 04 31 38.44      | +18 13 57.65     | $2360 \pm 90$  | CIDA-9 A           | 05 05 22.82      | +25 31 30.65     | $77 \pm 3$     |
| V710 Tau A       | 04 31 57.80      | +18 21 37.78     | $125 \pm 3$    | CIDA-9 B           | 05 05 22.97      | +25 31 31.84     | $< 7$          |
| V710 Tau B       | 04 31 57.81      | +18 21 34.61     | $< 10$         | RW Aur A           | 05 06 49.57      | +30 24 04.90     | $62 \pm 6$     |
| V710 Tau C       | 04 31 59.68      | +18 21 30.50     | $< 22$         | RW Aur B           | 05 06 49.47      | +30 24 04.53     | $9 \pm 5$      |
| GG Tau Ba        | 04 32 30.30      | +17 31 29.69     | $(< 7)$        |                    |                  |                  |                |

Note. — Col. (1): Stellar component name. Col. (2) and (3): Disk center coordinates. Col. (4):  $880 \mu\text{m}$  flux density. Values in parenthesis correspond to 1.3 mm. The sources in italics have  $F_d$  values from single-dish photometry (Andrews & Williams 2005).

Table 6. Properties of Stellar Pairs in Taurus

| System            | Pair           |                  | $\rho$<br>["] | $q$   | $M_p$<br>[ $M_\odot$ ] | $F_{\text{pair}}$<br>[mJy] | Refs   |
|-------------------|----------------|------------------|---------------|-------|------------------------|----------------------------|--|
|                   | Primary        | Secondary        |               |       |                        |                            |  |
| (1)               | (2)            | (3)              | (4)           | (5)   | (6)                    | (7)                        | (8)  |
| J04080782+2807280 | J04080782 A    | J04080782 B      | 0.044         | 0.13  | 0.30                   | (< 8)                      | 1, 1, A  |
| V773 Tau          | V773 Tau Aa    | V773 Tau Ab      | 0.0028        | 0.86  | 1.54                   | < 9                        | 2, 2, B <sup>a</sup>                             |
|                   | V773 Tau Aab   | V773 Tau B       | 0.14          | 0.29  | 2.87                   | < 9                        | 3, 3 <sup>b</sup> , B <sup>a</sup>               |
|                   | V773 Tau Aab   | V773 Tau C       | 0.21          | ...   | 2.87                   | < 9                        | 3, 3 <sup>b</sup> , B <sup>a</sup>               |
|                   | V773 Tau B     | V773 Tau C       | 0.20          | ...   | 1.33                   | < 9                        | 3 <sup>c</sup> , 3 <sup>b</sup> , B <sup>a</sup> |
|                   | V773 Tau ABC   | J0414118+2811535 | 23.38         | ~0.03 | > 4.20                 | (< 9)                      | 4, 1 <sup>b</sup> , A                            |
| Anon 1            | Anon 1 A       | Anon 1 B         | 0.015         | 0.68  | 0.64                   | < 8                        | 1, 1, B  |
| MHO 1/2           | MHO 1          | MHO 2 AB         | 3.93          | 1.00  | 0.44                   | (380 ± 3)                  | 4, 1, A  |
|                   | MHO 2 A        | MHO 2 B          | 0.050         | 0.34  | 0.33                   | (138 ± 1)                  | 1, 1, A  |
| MHO 3             | MHO 3 A        | MHO 3 B          | 0.031         | 0.81  | 0.72                   | (< 12)                     | 1, 1, A  |
| LkCa 3            | LkCa 3 Aa      | LkCa 3 Ab        | 0.0004        | 0.58  | 0.36                   | < 9                        | 5 <sup>c</sup> , 5 <sup>b</sup> , B              |
|                   | LkCa 3 Aab     | LkCa 3 B         | 0.48          | 0.81  | 0.57                   | < 9                        | 1, 1, B  |
| FO Tau            | FO Tau A       | FO Tau B         | 0.15          | 1.00  | 0.33                   | 13 ± 3                     | 1, 1, B  |
| LkCa 5            | LkCa 5 A       | LkCa 5 B         | 0.048         | 0.09  | 0.50                   | < 4                        | 1, 1, B  |
| V410 Tau          | V410 Tau A     | V410 Tau B       | 0.12          | 0.20  | 0.94                   | < 8                        | 1, 1, B <sup>a</sup>                             |
|                   | V410 Tau AB    | V410 Tau C       | 0.29          | 0.08  | 1.13                   | < 8                        | 1, 1, B <sup>a</sup>                             |
| DD Tau            | DD Tau A       | DD Tau B         | 0.55          | 1.00  | 0.33                   | 33 ± 4                     | 1, 1, A  |
| CZ Tau            | CZ Tau A       | CZ Tau B         | 0.32          | 0.50  | 0.54                   | < 9                        | 1, 1, B  |
| V410 Tau X-ray 7  | V410 X-ray 7 A | V410 X-ray 7 B   | 0.032         | 0.65  | 0.60                   | (< 13)                     | 1, 1, A  |
| Hubble 4          | Hubble 4 A     | Hubble 4 B       | 0.028         | 0.73  | 0.72                   | < 9                        | 1, 1, B  |
| FQ Tau            | FQ Tau A       | FQ Tau B         | 0.75          | 0.83  | 0.40                   | 8 ± 2                      | 1, 1, A  |
| LkCa 7            | LkCa 7 A       | LkCa 7 B         | 1.02          | 0.52  | 0.64                   | < 9                        | 1, 1, B  |
| T Tau             | T Tau Sa       | T Tau Sb         | 0.082         | 0.22  | 2.73                   | < 10                       | 6, 6, A <sup>a</sup>                             |
|                   | T Tau Sab      | T Tau N          | 0.68          | 0.63  | 3.34                   | 304 ± 3                    | 6 <sup>d</sup> , 6 <sup>b</sup> , A              |
| FS Tau            | FS Tau A       | FS Tau B         | 0.23          | 0.52  | 0.64                   | 49 ± 6                     | 1, 1, B  |
|                   | FS Tau AB      | Haro 6-5B        | 19.88         | 0.85  | 0.97                   | (155 ± 7)                  | 4, 1, B/C  |
| LkCa 21           | LkCa 21 A      | LkCa 21 B        | 0.044         | 0.77  | 0.41                   | < 10                       | 1, 1, B  |
| J1-4872           | J1-4872 Aa     | J1-4872 Ab       | 0.17          | 0.86  | 0.64                   | < 8                        | 1, 1, B  |
|                   | J1-4872 Ba     | J1-4872 Bb       | 0.10          | 0.67  | 0.59                   | < 8                        | 7, 7 <sup>b</sup> , B                            |
|                   | J1-4872 Aab    | J1-4872 Bab      | 3.38          | 0.83  | 1.19                   | < 8                        | 4, 1, B  |
| FV Tau            | FV Tau A       | FV Tau B         | 0.70          | 0.73  | 0.82                   | 26 ± 2                     | 1, 1, A  |
|                   | FV Tau/c A     | FV Tau/c B       | 0.70          | 0.73  | 0.45                   | < 5                        | 1, 1, A  |
|                   | FV Tau AB      | FV Tau/c AB      | 12.29         | 0.55  | 1.42                   | 26 ± 2                     | 4, 1, A  |
| DF Tau            | DF Tau A       | DF Tau B         | 0.073         | 0.90  | 0.50                   | 9 ± 2                      | 1, 1, B  |
| J1-507            | J1-507 A       | J1-507 B         | 0.079         | 0.98  | 0.27                   | < 6                        | 1, 1, B  |
| FW Tau            | FW Tau A       | FW Tau B         | 0.15          | 1.00  | 0.27                   | 5 ± 1                      | 1, 1, B  |
| DI/DH Tau         | DI Tau A       | DI Tau B         | 0.12          | 0.13  | 0.64                   | < 10                       | 1, 1, A  |
|                   | DH Tau A       | DH Tau B         | 2.34          | 0.07  | 0.57                   | 47 ± 4                     | 8, 8 <sup>b</sup> , A                            |
|                   | DI Tau AB      | DH Tau AB        | 15.23         | 0.85  | 0.72                   | 47 ± 4                     | 4, 1, A  |

Table 6—Continued

| System      | Primary      | Pair<br>Secondary | $\rho$<br>[ $''$ ] | $q$  | $M_p$<br>[ $M_\odot$ ] | $F_{\text{pair}}$<br>[mJy] | Refs                                  |
|-------------|--------------|-------------------|--------------------|------|------------------------|----------------------------|---------------------------------------|
| (1)         | (2)          | (3)               | (4)                | (5)  | (6)                    | (7)                        | (8)                                   |
| UX Tau      | UX Tau A     | UX Tau C          | 2.69               | 0.15 | 1.20                   | $141 \pm 1$                | 1, 1, A                               |
|             | UX Tau A     | UX Tau Bab        | 5.86               | 0.86 | 1.20                   | $141 \pm 1$                | 1, 1, A                               |
|             | UX Tau Ba    | UX Tau Bb         | 0.14               | 0.81 | 0.57                   | $< 3$                      | 1, 1, A                               |
|             | UX Tau Bab   | UX Tau C          | 6.45               | 0.17 | 1.03                   | $< 3$                      | 1, 1, A                               |
| FX Tau      | FX Tau A     | FX Tau B          | 0.89               | 0.47 | 0.57                   | $24 \pm 3$                 | 1, 1, A                               |
| DK Tau      | DK Tau A     | DK Tau B          | 2.34               | 0.89 | 0.64                   | $57 \pm 1$                 | 1, 1, A                               |
| ZZ Tau      | ZZ Tau A     | ZZ Tau B          | 0.042              | 0.48 | 0.40                   | $< 8$                      | 1, 1, B                               |
| V927 Tau    | V927 Tau A   | V927 Tau B        | 0.27               | 0.83 | 0.40                   | $< 10$                     | 1, 1, B                               |
| XZ/HL Tau   | XZ Tau A     | XZ Tau B          | 0.29               | 0.66 | 0.50                   | $(14 \pm 3)$               | 1, 1, C <sup>a</sup>                  |
|             | HL Tau       | XZ Tau AB         | 23.31              | 0.99 | 0.83                   | $2390 \pm 90$              | 4, 1, B                               |
| HK Tau      | HK Tau A     | HK Tau B          | 2.34               | 1.00 | 0.57                   | $130 \pm 3$                | 1, 1, A                               |
| V710 Tau    | V710 Tau A   | V710 Tau B        | 3.03               | 0.70 | 0.57                   | $125 \pm 3$                | 4, 1, A                               |
|             | V710 Tau AB  | V710 Tau C        | 27.97              | 0.41 | 0.97                   | $125 \pm 3$                | 4, 1, A                               |
| V827 Tau    | V827 Tau A   | V827 Tau B        | 0.093              | 0.63 | 0.72                   | $< 6$                      | 1, 1, B                               |
| V826 Tau    | V826 Tau A   | V826 Tau B        | 0.014              | 1.00 | 0.80                   | $< 7$                      | 9 <sup>c</sup> , 9 <sup>c</sup> , B   |
| V928 Tau    | V928 Tau A   | V928 Tau B        | 0.20               | 0.95 | 0.60                   | $< 8$                      | 1, 1, B                               |
|             | V928 Tau AB  | CFHT-Tau-7        | 18.25              | 0.10 | 1.17                   | $< 8$                      | 4, 1, B                               |
| GG Tau      | GG Tau Aa    | GG Tau Ab         | 0.24               | 0.83 | 0.72                   | $(557 \pm 3)$              | 1, 1, A                               |
|             | GG Tau Ba    | GG Tau Bb         | 1.48               | 0.31 | 0.11                   | $(< 5)$                    | 10, 10 <sup>b</sup> , A               |
|             | GG Tau Aab   | GG Tau Bab        | 10.38              | 0.14 | 1.32                   | $(557 \pm 3)$              | 4, 1, A                               |
| FZ/FY Tau   | FZ Tau       | FY Tau            | 17.17              | 0.89 | 0.72                   | $29 \pm 7$                 | 4, 1, B                               |
| UZ Tau      | UZ Tau Ea    | UZ Tau Eb         | 0.0009             | 0.30 | 1.05                   | $367 \pm 3$                | 11 <sup>c</sup> , 11 <sup>c</sup> , A |
|             | UZ Tau Wa    | UZ Tau Wb         | 0.37               | 0.80 | 0.50                   | $65 \pm 3$                 | 12, 12, A                             |
|             | UZ Tau Eab   | UZ Tau Wab        | 3.56               | 0.66 | 1.36                   | $432 \pm 4$                | 4, 1, A                               |
| JH 112      | JH 112 Aa    | JH 112 Ab         | 1.52               | 0.02 | 0.82                   | $15 \pm 4$                 | 1, 1, A                               |
|             | JH 112 Aab   | JH 112 B          | 6.56               | 0.31 | 0.83                   | $15 \pm 4$                 | 4, 1, A                               |
| V807/GH Tau | V807 Tau A   | V807 Tau Bab      | 0.28               | 0.62 | 0.72                   | $20 \pm 3$                 | 13, 13, B                             |
|             | V807 Tau Ba  | V807 Tau Bb       | 0.037              | ...  | $< 0.45$               | ...                        | 13, 13                                |
|             | GH Tau A     | GH Tau B          | 0.30               | 1.00 | 0.50                   | $15 \pm 3$                 | 1, 1, B                               |
|             | V807 Tau AB  | GH Tau AB         | 21.77              | 0.53 | 1.89                   | $35 \pm 4$                 | 4, 1, B                               |
| GI/GK Tau   | GI Tau       | GK Tau            | 13.14              | 1.00 | 0.72                   | $(15 \pm 1)$               | 4, 1, A                               |
| IS Tau      | IS Tau A     | IS Tau B          | 0.22               | 0.52 | 0.64                   | $30 \pm 3$                 | 1, 1, B                               |
| HN Tau      | HN Tau A     | HN Tau B          | 3.10               | 0.27 | 0.82                   | $34 \pm 3$                 | 4, 1, A                               |
| IT Tau      | IT Tau A     | IT Tau B          | 2.41               | 0.29 | 0.94                   | $27 \pm 4$                 | 1, 1, A                               |
| J2-2041     | J2-2041 A    | J2-2041 B         | 0.42               | 0.41 | 0.33                   | $< 19$                     | 1, 1, B                               |
| HBC 407     | HBC 407 A    | HBC 407 B         | 0.14               | 0.44 | 2.08                   | $< 14$                     | 1, 1, B                               |
| FF Tau      | FF Tau A     | FF Tau B          | 0.037              | 0.44 | 0.72                   | $< 4$                      | 1, 1, B                               |
| HBC 412     | HBC 412 A    | HBC 412 B         | 0.70               | 1.00 | 0.50                   | $< 9$                      | 1, 1, B                               |
| CoKu Tau/3  | CoKu Tau/3 A | CoKu Tau/3 B      | 2.07               | 0.17 | 0.57                   | $< 8$                      | 1, 1, B                               |



Table 6—Continued

| System              | Primary                | Pair<br>Secondary      | $\rho$<br>["] | $q$  | $M_p$<br>[ $M_\odot$ ] | $F_{\text{pair}}$<br>[mJy] | Refs                    |
|---------------------|------------------------|------------------------|---------------|------|------------------------|----------------------------|-------------------------|
| (1)                 | (2)                    | (3)                    | (4)           | (5)  | (6)                    | (7)                        | (8)                     |
| HP Tau              | HP Tau/G2              | HP Tau/G3 AB           | 10.09         | 0.38 | 2.49                   | (< 4)                      | 4, 1, A                 |
|                     | HP Tau/G2              | HP Tau                 | 21.30         | 0.38 | 2.49                   | (48 ± 2)                   | 4, 1, A                 |
|                     | HP Tau                 | HP Tau/G3 AB           | 16.70         | 1.00 | 0.95                   | (48 ± 2)                   | 4, 1, A                 |
|                     | HP Tau/G3 A            | HP Tau/G3 B            | 0.030         | 0.31 | 0.72                   | (< 4)                      | 1, 1, A                 |
| Haro 6-28           | Haro 6-28 A            | Haro 6-28 B            | 0.65          | 0.66 | 0.50                   | 11 ± 3                     | 1, 1, B                 |
| HV Tau              | HV Tau A               | HV Tau B               | 0.036         | 0.61 | 0.57                   | < 7                        | 4, 1, A                 |
|                     | HV Tau AB              | HV Tau C               | 3.98          | 0.78 | 0.92                   | 98 ± 3                     | 4, 1, A                 |
| VY Tau              | VY Tau A               | VY Tau B               | 0.66          | 0.29 | 0.64                   | < 10                       | 1, 1, B                 |
| GN Tau              | GN Tau A               | GN Tau B               | 0.34          | 0.87 | 0.45                   | 12 ± 3                     | 1, 1, B                 |
| JH 223              | JH 223 A               | JH 223 B               | 2.07          | 0.11 | 0.50                   | < 7                        | 1, 1, B                 |
| IW Tau              | IW Tau A               | IW Tau B               | 0.29          | 0.93 | 0.72                   | < 9                        | 1, 1, B                 |
| CoKu Tau/4          | CoKu Tau/4 A           | CoKu Tau/4 B           | 0.054         | 0.82 | 0.54                   | 9 ± 3                      | 1, 1, B                 |
| J04414565+2301580   | J04414565 Aa           | J04414565 Ab           | 0.22          | 0.10 | 0.40                   | < 24                       | 1, 1, A                 |
|                     | J04414565 Aab          | J04414565 B            | 12.37         | 0.06 | 0.44                   | < 24                       | 4, 1, A                 |
| LkH $\alpha$ 332    | LkH $\alpha$ 332/G2 A  | LkH $\alpha$ 332/G2 B  | 0.23          | 0.64 | 0.72                   | < 9                        | 1, 1, B                 |
|                     | LkH $\alpha$ 332/G1 A  | LkH $\alpha$ 332/G1 B  | 0.24          | 0.55 | 0.57                   | 12 ± 3                     | 1, 1, B                 |
|                     | V955 Tau A             | V955 Tau B             | 0.32          | 0.63 | 0.72                   | 14 ± 2                     | 1, 1, B                 |
|                     | LkH $\alpha$ 332/G2 AB | V955 Tau AB            | 10.51         | 0.99 | 1.18                   | 14 ± 2                     | 4, 1, B                 |
|                     | LkH $\alpha$ 332/G2 AB | LkH $\alpha$ 332/G1 AB | 25.88         | 0.75 | 1.18                   | 12 ± 3                     | 4, 1, B                 |
| DP Tau              | DP Tau A               | DP Tau B               | 0.11          | 0.74 | 0.64                   | < 10                       | 1, 1, B                 |
| RX J0446.7+2459     | RX J0446 A             | RX J0446 B             | 0.051         | 0.47 | 0.27                   | (< 5)                      | 1, 1, D                 |
| DQ Tau              | DQ Tau A               | DQ Tau B               | 0.0004        | 0.97 | 0.65                   | 208 ± 8                    | 14 <sup>c</sup> , 14, B |
| Haro 6-37           | Haro 6-37 Aa           | Haro 6-37 Ab           | 0.33          | 0.11 | 0.72                   | < 15                       | 1, 1, A                 |
|                     | Haro 6-37 Aab          | Haro 6-37 B            | 2.62          | 0.90 | 0.80                   | 218 ± 6                    | 1, 1, A                 |
| UY Aur              | UY Aur A               | UY Aur B               | 0.88          | 0.70 | 0.64                   | 49 ± 4                     | 1, 1, A                 |
| St 34               | St 34 Aa               | St 34 Ab               | < 0.01        | 1.00 | 0.40                   | < 11                       | 15, 15, B               |
|                     | St 34 Aab              | St 34 B                | 1.18          | 0.20 | 0.80                   | < 11                       | 1, 1, B                 |
| J04554757/J04554801 | J04554757+3028077      | J04554801+3028050      | 6.31          | 0.70 | 0.20                   | < 23                       | 4, 1, A                 |
| HBC 427             | HBC 427 A              | HBC 427 B              | 0.032         | 0.49 | 1.45                   | < 14                       | 1, 1, B                 |
| CIDA-9              | CIDA-9 A               | CIDA-9 B               | 2.34          | 0.58 | 0.72                   | 77 ± 3                     | 1, 1, A                 |
| CIDA-10             | CIDA-10 A              | CIDA-10 B              | 0.083         | 0.99 | 0.27                   | < 11                       | 1, 1, B                 |
| CIDA-11             | CIDA-11 A              | CIDA-11 B              | 0.097         | 0.76 | 0.27                   | < 8                        | 1, 1, B                 |
| RW Aur              | RW Aur A               | RW Aur B               | 1.38          | 0.60 | 1.20                   | 71 ± 8                     | 1, 1, A                 |

Note. — Col. (1): System name. Col (2): Primary designation of specified pair (note that this can consist of more than one star; see §2). Col. (3): Secondary designation of specified pair. Col. (4): Angular separation of the pair. Col. (5): Mass ratio of the pair ( $q = M_s/M_p$ ). Col. (6): Estimated stellar mass of the primary component of the pair. Col. (7): Composite 880  $\mu\text{m}$  flux density or upper limit for the pair. Values in parenthesis were measured instead at 1.3 mm: the analysis in §5 assumes a conservative scaling by a factor  $(1.3/0.88)^2 \approx 2.2$ . Col. (8): References for  $\rho$ ,  $q$ ,

and  $F_{\text{pair}}$ : [1] = Kraus et al. (2011), [2] = Boden et al. (2007), [3] = Duchêne et al. (2003), [4] = Kraus & Hillenbrand (2009b), [5] = Mathieu (1994), [6] = Duchêne et al. (2006), [7] = Correia et al. (2006), [8] = Itoh et al. (2005), [9] = Massarotti et al. (2005), [10] = White et al. (1999), [11] = Jensen et al. (2007), [12] = Kraus & Hillenbrand (2009a), [13] = Schaefer et al. (2006), [14] = Mathieu et al. (1997), [15] = White & Hillenbrand (2005), and [A] = this article, [B] = Andrews & Williams (2005), [C] = Osterloh & Beckwith (1995), [D] = Schaefer et al. (2009).

<sup>a</sup>The marginal detections of millimeter emission in the V773 Tau and V410 Tau systems by Andrews & Williams (2005) are likely unrelated to circumstellar dust. Both systems are known to emit relatively strong synchrotron radio signals Massi et al. (2006); Bieging et al. (1984). To be conservative, we consider these systems to have only upper limits on their millimeter luminosities. Synchrotron contamination from T Tau Sab is also likely to dominate over thermal emission from dust, even at millimeter wavelengths (see Loinard et al. 2007). The millimeter emission from the XZ Tau binary may also be contaminated, given its relatively bright centimeter-wave signal Carrasco-González et al. (see 2009). Moriarty-Schieven et al. (2006) suggest a smaller 880  $\mu\text{m}$  flux density of  $\sim 10$  mJy.

<sup>b</sup>The V773 Tau A-B mass ratio was computed assuming the V773 Tau Aab system mass from Boden et al. (2007). V773 Tau C is an “infrared companion” (Duchêne et al. 2003), so there are no reliable estimates of its mass to compute  $q$ . The total mass of LkCa 3 Aab estimated by Kraus et al. (2011) was used to help determine the mass ratio of the spectroscopic binary. The Duchêne et al. (2006) results were used in conjunction with the measurements of White & Ghez (2001) to estimate the T Tau Sab-N mass ratio. The DH Tau AB and GG Tau Bab mass ratios implicitly assume the  $M_p$  values derived by Kraus et al. (2011). The mass ratio for J1-4872 Bab was estimated from the spectral type and K-band magnitude difference from Correia et al. (2006), as described by Kraus et al. (2011).

<sup>c</sup>The single-lined spectroscopic binaries LkCa 3 Aab and UZ Tau Eab have a separation weighted by an unknown factor of  $\sin i$  and a mass ratio proportional to  $(\sin i)^3$  (although an independent inclination estimate is available for UZ Tau Eab, assuming its gas disk is co-planar; see Simon et al. 2000). The double-lined spectroscopic binaries V826 Tau AB and DQ Tau have only their separations weighted by  $\sin i$ ; the mass ratios are determined precisely. White & Hillenbrand (2005) demonstrated that St 34 Aab is a single-lined spectroscopic binary, but did not have sufficient radial velocity data to constrain the orbit. The V773 Tau B-C projected separation was estimated using the weighted mean position offsets at the same epochs from Duchêne et al. (2003).

<sup>d</sup>Although the current projected separation for the T Tau Sab-N pair is  $\sim 0''.7$  (Duchêne et al. 2006), astrometric monitoring of the pair suggests that the true separation is likely substantially larger. Köhler et al. (2008) suggest that the pair may be near periastron on an eccentric orbit with a much larger true separation,  $a \sim 1500$  AU, than would be suggested by the projected distance on the sky. In the analysis of §5, we adopt their estimate, but note that the major features of our statistical analysis do not depend on that decision.

Table 7. Single Stars Observed at Millimeter Wavelengths

| Name             | $M_*$         | $F_d$          | Ref  | Name            | $M_*$         | $F_d$        | Ref    |
|------------------|---------------|----------------|------|-----------------|---------------|--------------|--------|
| (1)              | [ $M_\odot$ ] | [mJy]          | (4)  | (1)             | [ $M_\odot$ ] | [mJy]        | (4)    |
| LkCa 1           | 0.27          | < 8            | 1, A | L1551-55        | 0.72          | < 5          | 1, A   |
| IRAS 04108+2910  | 0.30          | (< 20)         | 1, B | V830 Tau        | 0.72          | < 6          | 1, A   |
| FM Tau           | 0.64          | $32 \pm 8$     | 1, A | IRAS 04301+2608 | 0.64          | $18 \pm 6$   | 1, A   |
| CW Tau           | 0.94          | $66 \pm 6$     | 1, A | DL Tau          | 0.72          | $440 \pm 40$ | 1, A   |
| FP Tau           | 0.27          | (< 9)          | 1, B | DM Tau          | 0.57          | $210 \pm 1$  | 1, E   |
| CX Tau           | 0.45          | $25 \pm 6$     | 1, A | CI Tau          | 0.72          | $324 \pm 6$  | 1, A   |
| LkCa 4           | 0.72          | < 4            | 1, A | JH 108          | 0.57          | < 7          | 1, A   |
| CY Tau           | 0.57          | $140 \pm 5$    | 1, A | AA Tau          | 0.72          | $144 \pm 5$  | 1, A   |
| V410 Tau X-ray 1 | 0.30          | < 9            | 1, C | HO Tau          | 0.60          | $44 \pm 6$   | 1, A   |
| HBC 372          | 0.94          | < 8            | 1, A | DN Tau          | 0.64          | $201 \pm 7$  | 1, A   |
| HBC 376          | 0.72          | < 6            | 1, A | HQ Tau          | 0.94          | $11 \pm 3$   | 1, A   |
| BP Tau           | 0.72          | $130 \pm 7$    | 1, A | LkCa 14         | 0.64          | < 9          | 1, A   |
| V819 Tau         | 0.72          | < 9            | 1, A | DO Tau          | 0.64          | $258 \pm 42$ | 1, A   |
| DE Tau           | 0.50          | $90 \pm 7$     | 1, A | LkCa 15         | 1.01          | $410 \pm 1$  | 1, E   |
| RY Tau           | 1.46          | $560 \pm 30$   | 1, A | ITG 33A         | 0.40          | (< 5)        | 1, B   |
| HD 283572        | 2.26          | < 9            | 1, A | IRAS 04385+2550 | 0.64          | $(24 \pm 1)$ | 1, B   |
| FT Tau           | 0.60          | $121 \pm 5$    | 1, A | GO Tau          | 0.64          | $173 \pm 7$  | 1, A   |
| IRAS 04216+2603  | 0.64          | (< 20)         | 1, B | DR Tau          | 0.72          | $533 \pm 7$  | 1, A   |
| IP Tau           | 0.64          | $34 \pm 5$     | 1, A | DS Tau          | 0.82          | $39 \pm 4$   | 1, A   |
| DG Tau           | 0.94          | $1100 \pm 100$ | 1, A | Haro 6-39       | ...           | $36 \pm 6$   | ..., A |
| IRAS 04260+2642  | 0.94          | $(105 \pm 10)$ | 1, D | GM Aur          | 0.94          | $640 \pm 4$  | 1, E   |
| HBC 388          | 1.46          | < 6            | 1, A | LkCa 19         | 1.69          | < 10         | 1, A   |
| IQ Tau           | 0.60          | $178 \pm 3$    | 1, A | SU Aur          | 2.34          | $74 \pm 3$   | 1, A   |
| JH 56            | 0.60          | < 8            | 1, A | V836 Tau        | 0.72          | $74 \pm 3$   | 1, A   |
| L1551-51         | 0.72          | < 13           | 1, A | CIDA-8          | 0.33          | $27 \pm 3$   | 1, A   |
| Haro 6-13        | 0.64          | $395 \pm 56$   | 1, A | CIDA-12         | 0.27          | < 7          | 1, A   |

Note. — Col. (1): Star name. Col. (2): Estimated stellar mass. Col. (3):  $880 \mu\text{m}$  flux density or upper limit. Values in parenthesis were measured instead at 1.3 mm: the analysis in §5 assumes a conservative scaling by a factor  $(1.3/0.88)^2 \approx 2.2$ . Col. (4): References for  $M_*$  and  $F_d$ : [1] = Kraus et al. (2011), and [A] = Andrews & Williams (2005), [B] = Schaefer et al. (2009), [C] = Motte & André (2001), [D] = Mannings & Emerson (1994), and [E] = Andrews et al. (2011).

Table 8. Millimeter Detection Statistics

| Type          | $N_{\text{det}}$ | $N_{\text{tot}}$ | $f_{\text{mm}}$  |
|---------------|------------------|------------------|------------------|
| singles       | 32               | 52               | $62 \pm 11\%$    |
| binaries      | 26-34            | 96               | $27-35 \pm 5\%$  |
| triples       | 11-15            | 39               | $28-38 \pm 10\%$ |
| higher order  | 13-18            | 44               | $30-41 \pm 10\%$ |
| all multiples | 50-67            | 179              | $28-37 \pm 5\%$  |

Note. — Col. (1): Type of stellar system. Col. (2): Number of individual stars with detected millimeter emission. Col. (3): Total number of stars of that category. Col. (4): Millimeter detection fraction.

Table 9. Two-Sample Tests Comparing Millimeter Luminosity Distributions

| Group 1                        | Group 2                       | $\mathcal{P}(\text{survival})$ | $\mathcal{P}(\text{K-S})$ |
|--------------------------------|-------------------------------|--------------------------------|---------------------------|
| single stars                   | wide pairs (>300 AU)          | 0.20-0.40                      | 0.37                      |
| wide pairs (>300 AU)           | medium pairs (30-300 AU)      | <0.00006                       | 0.017                     |
| medium pairs (30-300 AU)       | small pairs (<30 AU)          | <0.00005                       | 0.047                     |
| high mass ratios ( $q > 0.5$ ) | low mass ratios ( $q < 0.5$ ) | <0.04                          | 0.48                      |
| wide pairs with $q > 0.5$      | wide pairs with $q < 0.5$     | <0.00001                       | 0.77                      |
| medium pairs with $q > 0.5$    | medium pairs with $q < 0.5$   | <0.08                          | 0.10                      |
| single stars                   | primaries in pairs            | 0.41-0.98                      | ...                       |
| primaries in pairs             | secondaries in pairs          | <0.008                         | ...                       |

Note. — Cols. (1) & (2): The sub-populations being compared. Col. (3): The probability that these two groups are drawn from the same parent distributions. The listed values correspond to the range or more conservative limit from the standard two-sample tests used in survival analysis (Peto-Prentice, Logrank, and Gehan tests). Col. (4): Same as Col. (3), but for the special case that includes only those pairs with millimeter-wave detections in each sub-population, derived from the two-sided Kolmogorov-Smirnov test.

## REFERENCES

- Abt, H. A., & Levy, S. G. 1976, *ApJS*, 30, 273
- Akeson, R. L., Koerner, D. W., & Jensen, E. L. N. 1998, *ApJ*, 505, 358
- Akeson, R. L., Rice, W. K. M., Boden, A. F., et al. 2007, *ApJ*, 670, 1240
- Ambartsumian, V. A. 1937, *AZh*, 14, 207
- Andrews, S. M., Czekala, I., Wilner, D. J., et al. 2010, *ApJ*, 710, 462
- Andrews, S. M., & Williams, J. P. 2005, *ApJ*, 631, 1134
- . 2007a, *ApJ*, 671, 1800
- . 2007b, *ApJ*, 659, 705
- Andrews, S. M., Wilner, D. J., Espaillat, C., et al. 2011, *ApJ*, 732, 42
- Andrews, S. M., Wilner, D. J., Hughes, A. M., et al. 2012, *ApJ*, 744, 162
- Artymowicz, P., & Lubow, S. H. 1994, *ApJ*, 421, 651
- Baraffe, I., Chabrier, G., Allard, F., & Hauschildt, P. H. 1998, *A&A*, 337, 403
- Bate, M. R., & Bonnell, I. A. 1997, *MNRAS*, 285, 33
- Beckwith, S. V. W., Sargent, A. I., Chini, R. S., & Guesten, R. 1990, *AJ*, 99, 924
- Beust, H., & Dutrey, A. 2005, *A&A*, 439, 585
- Biegging, J. H., Cohen, M., & Schwartz, P. R. 1984, *ApJ*, 282, 699
- Boden, A. F., Torres, G., Sargent, A. I., et al. 2007, *ApJ*, 670, 1214
- Bonavita, M., & Desidera, S. 2007, *A&A*, 468, 721
- Bonnell, I. A., & Bate, M. R. 1994, *MNRAS*, 269, L45
- Carrasco-González, C., Rodríguez, L. F., Anglada, G., & Curiel, S. 2009, *ApJ*, 693, L86
- Cieza, L. A., Padgett, D. L., Allen, L. E., et al. 2009, *ApJ*, 696, L84
- Correia, S., Zinnecker, H., Ratzka, T., & Sterzik, M. F. 2006, *A&A*, 459, 909
- Desidera, S., & Barbieri, M. 2007, *A&A*, 462, 345
- Desidera, S., Carolo, E., Gratton, R., et al. 2011, *A&A*, 533, A90
- Doyle, L. R., Carter, J. A., Fabrycky, D. C., et al. 2011, *Science*, 333, 1602

- Duchêne, G. 2010, *ApJ*, 709, L114
- Duchêne, G., Beust, H., Adjali, F., Konopacky, Q. M., & Ghez, A. M. 2006, *A&A*, 457, L9
- Duchêne, G., Delgado-Donate, E., Haisch, Jr., K. E., Loinard, L., & Rodríguez, L. F. 2007, *Protostars and Planets V*, 379
- Duchêne, G., Ghez, A. M., McCabe, C., & Weinberger, A. J. 2003, *ApJ*, 592, 288
- Dupuy, T. J., & Liu, M. C. 2011, *ApJ*, 733, 122
- Duquennoy, A., & Mayor, M. 1991, *A&A*, 248, 485
- Feigelson, E. D., & Nelson, P. I. 1985, *ApJ*, 293, 192
- Fischer, D. A., & Marcy, G. W. 1992, *ApJ*, 396, 178
- Ghez, A. M., Neugebauer, G., & Matthews, K. 1993, *AJ*, 106, 2005
- Guilloteau, S., Dutrey, A., & Simon, M. 1999, *A&A*, 348, 570
- Hartmann, L., Calvet, N., Gullbring, E., & D'Alessio, P. 1998, *ApJ*, 495, 385
- Ho, P. T. P., Moran, J. M., & Lo, K. Y. 2004, *ApJ*, 616, L1
- Hughes, A. M., Wilner, D. J., Qi, C., & Hogerheijde, M. R. 2008, *ApJ*, 678, 1119
- Itoh, Y., Hayashi, M., Tamura, M., et al. 2005, *ApJ*, 620, 984
- Jensen, E. L. N., & Akeson, R. L. 2003, *ApJ*, 584, 875
- Jensen, E. L. N., Dhital, S., Stassun, K. G., et al. 2007, *AJ*, 134, 241
- Jensen, E. L. N., Koerner, D. W., & Mathieu, R. D. 1996a, *AJ*, 111, 2431
- Jensen, E. L. N., Mathieu, R. D., Donar, A. X., & Dullighan, A. 2004, *ApJ*, 600, 789
- Jensen, E. L. N., Mathieu, R. D., & Fuller, G. A. 1994, *ApJ*, 429, L29
- . 1996b, *ApJ*, 458, 312
- Köhler, R., Ratzka, T., Herbst, T. M., & Kasper, M. 2008, *A&A*, 482, 929
- Kraus, A. L., & Hillenbrand, L. A. 2009a, *ApJ*, 704, 531
- . 2009b, *ApJ*, 703, 1511
- Kraus, A. L., Ireland, M. J., Hillenbrand, L. A., & Martinache, F. 2012, *ArXiv e-prints*
- Kraus, A. L., Ireland, M. J., Martinache, F., & Hillenbrand, L. A. 2011, *ArXiv e-prints*

- Lada, C. J. 2006, *ApJ*, 640, L63
- Launhardt, R. 2004, in *IAU Symposium*, Vol. 221, *Star Formation at High Angular Resolution*, ed. M. G. Burton, R. Jayawardhana, & T. L. Bourke, 213
- Leinert, C., Zinnecker, H., Weitzel, N., et al. 1993, *A&A*, 278, 129
- Lin, D. N. C., & Papaloizou, J. 1979a, *MNRAS*, 188, 191
- . 1979b, *MNRAS*, 186, 799
- Loinard, L., Torres, R. M., Mioduszewski, A. J., et al. 2007, *ApJ*, 671, 546
- Luhman, K. L., Allen, P. R., Espaillat, C., Hartmann, L., & Calvet, N. 2010, *ApJS*, 186, 111
- Mannings, V., & Emerson, J. P. 1994, *MNRAS*, 267, 361
- Markwardt, C. B. 2009, in *Astronomical Society of the Pacific Conference Series*, Vol. 411, *Astronomical Data Analysis Software and Systems XVIII*, ed. D. A. Bohlender, D. Durand, & P. Dowler, 251
- Massarotti, A., Latham, D. W., Torres, G., Brown, R. A., & Oppenheimer, B. D. 2005, *AJ*, 129, 2294
- Massi, M., Forbrich, J., Menten, K. M., et al. 2006, *A&A*, 453, 959
- Mathieu, R. D. 1994, *ARA&A*, 32, 465
- Mathieu, R. D., Ghez, A. M., Jensen, E. L. N., & Simon, M. 2000, *Protostars and Planets IV*, 703
- Mathieu, R. D., Stassun, K., Basri, G., et al. 1997, *AJ*, 113, 1841
- McCabe, C., Duchêne, G., Pinte, C., et al. 2011, *ApJ*, 727, 90
- Melo, C. H. F., Covino, E., Alcalá, J. M., & Torres, G. 2001, *A&A*, 378, 898
- Moriarty-Schieven, G. H., Johnstone, D., Bally, J., & Jenness, T. 2006, *ApJ*, 645, 357
- Motte, F., & André, P. 2001, *A&A*, 365, 440
- Mugrauer, M., & Neuhäuser, R. 2009, *A&A*, 494, 373
- Mundy, L. G., Looney, L. W., Erickson, W., et al. 1996, *ApJ*, 464, L169
- Nagel, E., D'Alessio, P., Calvet, N., et al. 2010, *ApJ*, 708, 38
- Ochi, Y., Sugimoto, K., & Hanawa, T. 2005, *ApJ*, 623, 922
- Osterloh, M., & Beckwith, S. V. W. 1995, *ApJ*, 439, 288

- Panić, O., Hogerheijde, M. R., Wilner, D., & Qi, C. 2009, *A&A*, 501, 269
- Papaloizou, J., & Pringle, J. E. 1977, *MNRAS*, 181, 441
- Patience, J., Akeson, R. L., & Jensen, E. L. N. 2008, *ApJ*, 677, 616
- Patience, J., White, R. J., Ghez, A. M., et al. 2002, *ApJ*, 581, 654
- Pichardo, B., Sparke, L. S., & Aguilar, L. A. 2005, *MNRAS*, 359, 521
- Piétu, V., Gueth, F., Hily-Blant, P., Schuster, K.-F., & Pety, J. 2011, *A&A*, 528, A81
- Raghavan, D., Henry, T. J., Mason, B. D., et al. 2006, *ApJ*, 646, 523
- Raghavan, D., McAlister, H. A., Henry, T. J., et al. 2010, *ApJS*, 190, 1
- Reipurth, B., & Zinnecker, H. 1993, *A&A*, 278, 81
- Richichi, A., Köhler, R., Woitas, J., & Leinert, C. 1999, *A&A*, 346, 501
- Schaefer, G. H., Dutrey, A., Guilloteau, S., Simon, M., & White, R. J. 2009, *ApJ*, 701, 698
- Schaefer, G. H., Simon, M., Beck, T. L., Nelan, E., & Prato, L. 2006, *AJ*, 132, 2618
- Scholz, A., Jayawardhana, R., & Wood, K. 2006, *ApJ*, 645, 1498
- Simon, M., Chen, W. P., Howell, R. R., Benson, J. A., & Slowik, D. 1992, *ApJ*, 384, 212
- Simon, M., Dutrey, A., & Guilloteau, S. 2000, *ApJ*, 545, 1034
- Simon, M., Ghez, A. M., Leinert, C., et al. 1995, *ApJ*, 443, 625
- Tokovinin, A. A. 1998, *Astronomy Letters*, 24, 178
- Torres, G. 1999, *PASP*, 111, 169
- Torres, R. M., Loinard, L., Mioduszewski, A. J., & Rodríguez, L. F. 2007, *ApJ*, 671, 1813
- . 2009, *ApJ*, 698, 242
- Verrier, P. E., & Evans, N. W. 2008, *MNRAS*, 390, 1377
- White, R. J., & Ghez, A. M. 2001, *ApJ*, 556, 265
- White, R. J., Ghez, A. M., Reid, I. N., & Schultz, G. 1999, *ApJ*, 520, 811
- White, R. J., & Hillenbrand, L. A. 2005, *ApJ*, 621, L65
- Zahn, J.-P. 1977, *A&A*, 57, 383
- Zahn, J.-P., & Bouchet, L. 1989, *A&A*, 223, 112